

## RESEARCH ARTICLE

# Reduction of endocytic activity accelerates cell elimination during tissue remodeling of the *Drosophila* epidermal epithelium

Shinichiro Hoshika, Xiaofei Sun, Erina Kuranaga\* and Daiki Umetsu\*

## ABSTRACT

Epithelial tissues undergo cell turnover both during development and for homeostatic maintenance. Cells that are no longer needed are quickly removed without compromising the barrier function of the tissue. During metamorphosis, insects undergo developmentally programmed tissue remodeling. However, the mechanisms that regulate this rapid tissue remodeling are not precisely understood. Here, we show that the temporal dynamics of endocytosis modulate physiological cell properties to prime larval epidermal cells for cell elimination. Endocytic activity gradually reduces as tissue remodeling progresses. This reduced endocytic activity accelerates cell elimination through the regulation of Myosin II subcellular reorganization, junctional E-cadherin levels, and caspase activation. Whereas the increased Myosin II dynamics accelerates cell elimination, E-cadherin plays a protective role against cell elimination. Reduced E-cadherin is involved in the amplification of caspase activation by forming a positive-feedback loop with caspase. These findings reveal the role of endocytosis in preventing cell elimination and in the cell-property switching initiated by the temporal dynamics of endocytic activity to achieve rapid cell elimination during tissue remodeling.

**KEY WORDS:** Endocytosis, Tissue remodeling, Epithelial cell elimination, Cell extrusion, Myosin II, E-cadherin, Caspase, *Drosophila*

## INTRODUCTION

Tissues and organs operate under the tight control of cell turnover in order to maintain tissue integrity and homeostasis throughout life. Multiple tissues in mammals, such as skin, the intestine and the mammary gland, are in a continuous renewal or regenerative state (Clevers et al., 2014) – old cells are constantly removed and newly differentiated cells take their place. Similar cell turnover has been also observed in cell competition, wherein cells with higher fitness replace less-fit cells (De La Cova et al., 2004; Moreno and Basler, 2004; Maruyama and Fujita, 2017; Ohsawa et al., 2018). These processes benefit organisms by allowing them not only to maintain tissue homeostasis but also to quickly respond to tissue injury or the emergence of unwanted cells via spontaneous mutation (Merino et al., 2016; Wells and Watt, 2018). Cell turnover also occurs during development. One conspicuous instance is that of metamorphosis in insects. In contrast to homeostatic cell turnover, the replacement of


cells during metamorphosis takes place only once, and the cells in the entire tissue undergo massive cell death. Despite its fundamental role in development, the precise mechanism that regulates this rapid cell elimination remains elusive.

Proper control of cell extrusion is crucial for tissue remodeling because the misregulation of this process can lead to tumorigenesis, due to loss of contact inhibition, and to bacterial infection caused by defects in the first-line barrier (Gudipaty and Rosenblatt, 2017; Ohsawa et al., 2018). The development of the *Drosophila* abdomen epidermis serves as a good model system for understanding the molecular and cellular dynamics involved in tissue remodeling (Ninov et al., 2007; Nakajima et al., 2011). The adult epidermis is derived from discrete cell populations called histoblast nests, which consist of imaginal cells and are embedded in the larval epidermal tissue (Fig. 1A). Larval epidermal cells (LECs) are squamous large polyploid cells (up to 70  $\mu\text{m}$  in diameter) that cover the epidermis of the larval abdomen (Madhavan and Madhavan, 1980; Bischoff, 2012). The tissue remodeling process completes within 20 h, and the LECs that originally cover the whole tissue are completely replaced by histoblasts (Fig. 1A). Histoblasts remain mitotically quiescent from the embryo stage to the onset of the pupal stage (Roseland and Schneiderman, 1979). Then, histoblasts undergo massive cell proliferation during the pupal stage at the expense of the LECs (Madhavan and Madhavan, 1980). Despite such a drastic and rapid remodeling of the tissue, the coordination between the elimination of LECs and the expansion of histoblasts typically proceeds without compromising the tissue integrity or barrier function of the tissue (Gudipaty and Rosenblatt, 2017). The way that cells are removed from the tissue helps to protect the tissue integrity (Lubkov and Barsagi, 2014). The elimination of cells is executed by means of apical constriction, whereby actomyosin cables formed at the cell cortex drive dramatic reduction of apical area (Ninov et al., 2007; Teng et al., 2017). During apical constriction-driven cell elimination, caspase activation regulates Myosin II accumulation and also contributes to junction remodeling (Teng et al., 2017). Activation of caspase before cell extrusion has been also shown in the context of cell competition (Levayer et al., 2016). However, it is still unclear how the temporal dynamics of cell elimination are controlled in developmentally programmed tissue remodeling.

Endocytosis regulates various cellular activities, such as cell proliferation, differentiation and metabolism (Sigismund et al., 2012). Endocytosis initiates membrane trafficking, which then leads to the incorporation of ligands and signaling receptors together with membrane materials into vesicles to sort them to other intracellular compartments, such as recycling endosomes or lysosomes for protein degradation, which leads to shutting off of signaling. Some signaling pathways are activated by endocytosis whereas others are downregulated (Seto et al., 2002; Fischer et al., 2006). Endocytic defects in the signal transduction pathway regulation typically result in the inhibition of programmed cell death, suggesting a tumor-suppressive role, and more rarely in the induction of cell death

Laboratory for Histogenetic Dynamics, Department of Ecological Developmental Adaptability Life Sciences, Graduate School of Life Sciences, Tohoku University, Sendai, 980-8578, Japan.

\*Authors for correspondence (erina.kuranaga.d1@tohoku.ac.jp; umetsu@tohoku.ac.jp)

 S.H., 0000-0002-4473-9187; X.S., 0000-0003-2115-1951; E.K., 0000-0001-6300-2087; D.U., 0000-0002-1916-6903

Received 16 April 2019; Accepted 24 February 2020

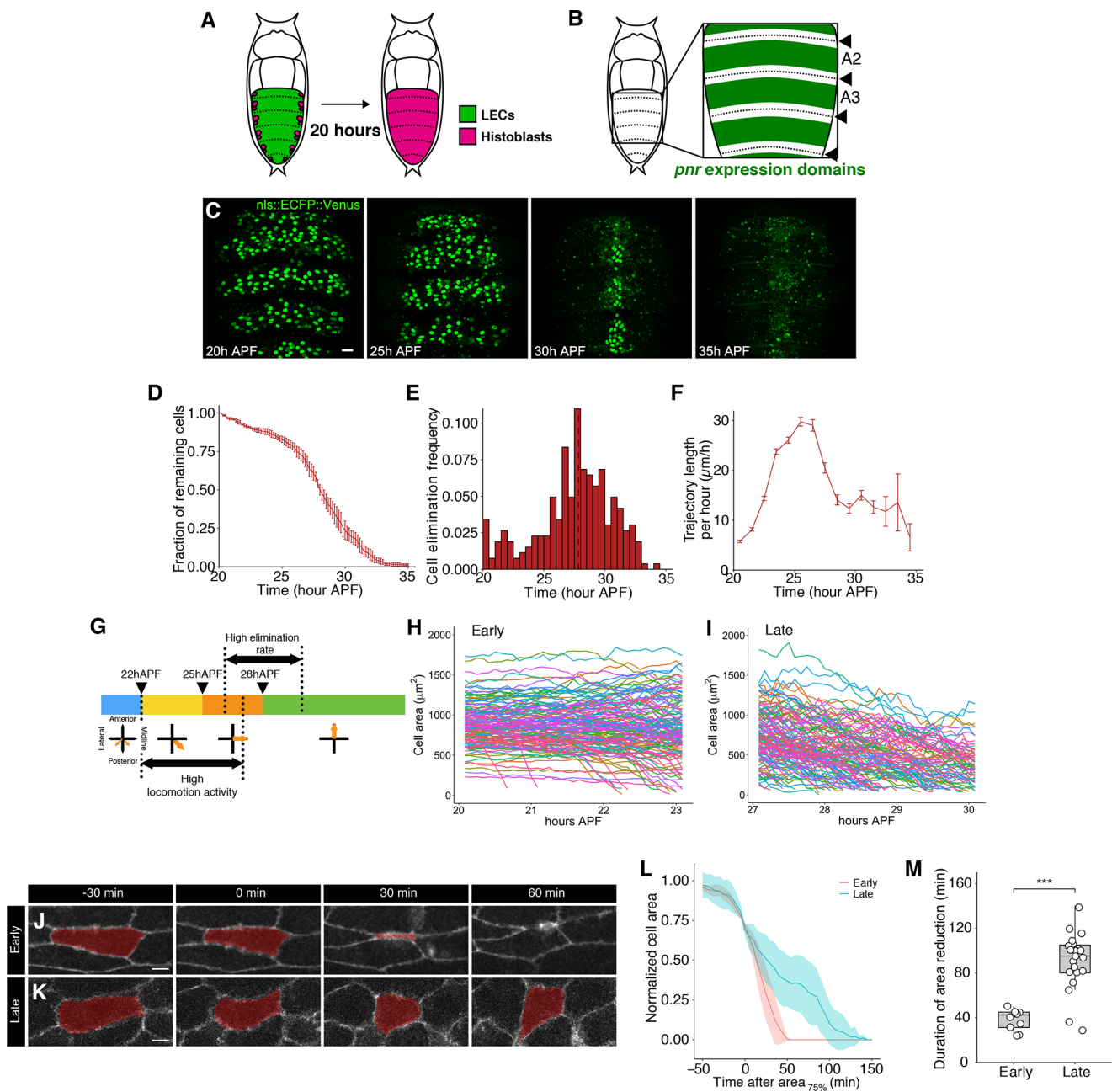


**Fig. 1. Cell elimination rate accelerates as tissue remodeling progresses.** (A) Schematic to illustrate tissue remodeling. Proliferating histoblasts (magenta) replace larval epidermal cells (LECs, green) during tissue remodeling. (B) Schematic to illustrate the *pnr*-GAL4 driver expression domains. Arrowheads indicate segment boundaries, and the *pnr*-GAL4 driver expression domains are shown in green. (C) Time course of the elimination of LECs that are labeled by nuclear-localized CFP::Venus under the control of the *pnr*-GAL4 driver at 25°C. Images were taken from a single time-lapse imaging movie. Anterior is up. Scale bar: 50  $\mu\text{m}$ . (D) Time course analysis of the number of remaining LECs normalized to the number at the first frame of the live imaging in the wild-type animal.  $n=2$  segments of 3 pupae. Error bars are s.e.m. (E) Histogram of the number of eliminated cells at each time point. Bin size is 0.5 h.  $n=2$  segments of 3 pupae, 263 cells. Dashed line indicates the median value. (F) The rate of LEC migration (average trajectory length within an hour) at each time point.  $n=2$  segments of 3 pupae. Error bars are s.e.m. (G) Timeline of the high elimination phase with respect to the migration pattern of the LECs at 25°C. Color code represents different developmental time windows from early to late stages based on the locomotion activity and orientation of migration. Times (hours after puparium formation) of transition are indicated at the top. Orange arrows indicate the orientation of the LEC migration at each time window. The time periods of high locomotion activity and high elimination rate are indicated below and above, respectively. (H,I) Area change of individual LECs (colors are for individual cell IDs) in a pupa at the late stage (H, 140 cells) and the late stage (I, 127 cells). (J,K) Images of area reduction for extruding LECs at the early (J) and late (K) stages labeled with an Nrg-GFP protein trap line. Scale bars: 10  $\mu\text{m}$ . (L) Mean area over time for extruding LECs during the early (red) and the late (blue) stages. Normalized cell areas are plotted against the time after each cell reaches 75% of its initial cell area. Shaded area represents s.d. (M) Duration of area reduction for extruding LECs during the early and late stages. Mann–Whitney *U*-test, \*\*\* $P<0.001$ .  $n=10$  cells, early stage;  $n=21$  cells, late stage.

(Moreno and Basler, 2004; Vaccari and Bilder, 2009; Twomey et al., 2015). Furthermore, endocytosis also acts at another hierarchical layer, having a more direct physical role in cell shape

change. During *Xenopus* gastrulation, for example, cells in the dorsal marginal zone undergo apical constriction, and this process is endocytosis dependent (Lee and Harland, 2010). Turnover of

adherens junction components are also dependent on endocytotic activity in epithelial tissues (Georgiou et al., 2008; Levayer et al., 2011; Jewett et al., 2017; Iyer et al., 2019). It is not known how endocytosis regulates cell elimination during tissue remodeling or whether endocytosis promotes apical constriction in this process.

In this study, we investigated the role of endocytosis in cell elimination during tissue remodeling in the *Drosophila* abdominal epidermis. We found that the tissue remodeling progresses in two phases: the early stage where LEC eliminations are sparse and the late stage where LEC eliminations are frequent. This transition is regulated by the gradual reduction of endocytic activity in the LECs. The reduction of endocytosis induces dynamic Myosin II accumulation and caspase activation. The caspase activation involves an amplification mechanism through positive feedback with junctional E-cadherin (Shotgun in *Drosophila*). Our data suggest that the temporal dynamics of endocytosis regulate Myosin II and E-cadherin to prime LECs for cell elimination.

## RESULTS

### Elimination of LECs during tissue remodeling proceeds in two phases

Developmental programs operate under tight temporal controls. The LECs in the pupal abdomen are quickly replaced by proliferating imaginal cells, the histoblasts, during metamorphosis (Fig. 1A) (Roseland and Schneiderman, 1979; Madhavan and Madhavan, 1980; Ninov et al., 2007). Previous work has identified that the LECs switch their character from stationary to migratory during tissue remodeling in the epidermis of the abdomen (Bischoff, 2012; Arata et al., 2017). To examine whether this transition parallels the temporal pattern of LEC elimination, we quantitatively analyzed the dynamics of cell elimination over the course of tissue remodeling via live imaging. We visualized the nuclei of LECs by expressing a fluorescent protein, Venus, under the control of the GAL4/UAS system using an LEC-specific driver, *pnr*-GAL4. *pnr*-GAL4 is strongly expressed in the middle of each segment, including both anterior and posterior compartment cells (Arata et al., 2017) (Fig. 1B). Individual nuclei were tracked, and the number of nuclei was counted at each time point. This approach allowed us to analyze both the length and orientation of individual cells' trajectories as well as the frequency of cell elimination in a systematic manner. We observed the nuclei from 20 h after puparium formation (APF), when the histoblasts start spreading, to 35 h APF, when the LECs are completely eliminated from the tissue (Fig. 1C, Movie 1) (Bischoff, 2012). We found that the rate of LEC elimination is not constant throughout the remodeling process. Rather, it began slowly and sped up at the later stages (Fig. 1D,E). The transition took place after the LECs reoriented their migration (27–28 h APF at 25°C) (Fig. 1F,G). In order to identify the cellular activity that regulates the transition of cell character over the course of the tissue remodeling, we decided to focus on the behavior of the LECs at the late stage (about 30 h APF at 25°C) compared with the early stage (about 20 h APF at 25°C), when the LECs have not yet started to migrate. By tracking the cell shape of LECs from the entire tissue, we found that the majority of LECs do not reduce their area in the early phase, but they showed an overall tendency to reduce the cell area during the late phase time window (Fig. 1H,I). In addition, the rate of cell area reduction was faster for the LECs eliminated during the early phase than the late phase, suggesting that the increased cell elimination rate at the late stage is not due to an increased area constriction speed of individual cells (Fig. 1J–M). In summary, these observations suggest that the LECs change property between the early and late stages.

### Endocytic activity in LECs is attenuated in the late stage, and the reduced endocytosis promotes cell elimination

In order to identify the cellular activity that triggers this transition from low to high cell elimination rate, we focused on the endocytic activity. Endocytosis plays diverse roles in epithelial development, including the control of cell death, apical constriction, and remodeling of adherens junctions (Classen et al., 2005; Georgiou et al., 2008; Igaki et al., 2009; Lee and Harland, 2010; Levayer et al., 2011; Saitoh et al., 2017; Iyer et al., 2019). Endocytosis regulates these processes either by regulating signal transduction pathways or through physical turnover of cell-cell junction components. To investigate whether endocytosis actively regulates LEC elimination, which involves those physical processes, we analyzed the long-term temporal evolution of endocytic activity by monitoring the clathrin light chain protein tagged with GFP (Clc-GFP) expressed under the control of *pnr*-GAL4. At the early stage, numerous Clc-GFP punctate structures were visible (Fig. 2A,C), but the number of puncta decreased at the late stage (Fig. 2B,C, Movie 2). To corroborate this result, we performed a dextran uptake assay that monitors fluid phase incorporation into intracellular vesicles. We found that the dextran uptake activity was also reduced over the course of the tissue remodeling process (Fig. S1D–E"). These results reveal an intriguing correlation between the reduction of endocytic activity and the increase in cell elimination rate, which is counterintuitive given the well-established roles of endocytosis in promoting cell death, apical constriction and junctional remodeling, all of which are involved in LEC elimination.

In order to test the possibility that the reduced endocytic activity promotes cell elimination of LECs, we genetically manipulated the Dynamin GTPase encoded by *shibire* (*shi*), which is required for pinching off clathrin-coated endocytic vesicles (Herskovits et al., 1993; Van der Blik et al., 1993). Using a temperature-sensitive, dominant-negative form of Dynamin (*shi*<sup>ts</sup>) (Grigliatti et al., 1973), we established a temperature shift regime during this tissue remodeling. Overexpression of *shi*<sup>ts</sup> in LECs using *pnr*-GAL4 dramatically reduced puncta of Clc-GFP as well as Dextran uptake under the restrictive temperature (Fig. S1A–B',F–G), confirming that *shi*<sup>ts</sup> efficiently blocks endocytosis in the LECs in a temperature-dependent manner. We next tested whether our temperature-shift regime affects the normal behavior of LECs by carefully examining normal tissue remodeling. As a reference, we used the LEC migration described previously (Bischoff, 2012; Arata et al., 2017). We found that the overall process was delayed, but LEC elimination still coordinated well with the temporal migration pattern observed at 25°C where LECs migrate initially posteriorly, then toward the midline, and finally anteriorly before all LECs were eliminated (Fig. 1D–G, Fig. S2A,B). The period of the high elimination rate occurred during midline-oriented migration, both at 25°C and under the temperature shift regime (compare Fig. 1G with Fig. S2D). Having established the minimal effect of the temperature shift on tissue remodeling, we refer to control experiments performed under restrictive temperature (RT) as RT control and examined the effect of endocytosis on LECs. Expression of *shi*<sup>ts</sup> caused LECs at the early stage to slow down the rate of area constriction to a similar extent to that observed at the late stage in RT control animals, suggesting that reduction in endocytic activity is the cause of the switch in LEC property (Fig. 2D,E). More importantly, the LECs expressing *shi*<sup>ts</sup> underwent frequent elimination even at the early stage, and the rate of cell elimination peaked earlier than in RT controls (Fig. 2F,G,I–K, Movie 3). The same effect was observed using another LEC-specific GAL4 driver, Eip71CD-GAL4, confirming the cell autonomous effect of blocking endocytic activity (Sekyrova et al., 2010; Teng et al., 2017) (Fig. S1H–J). These results



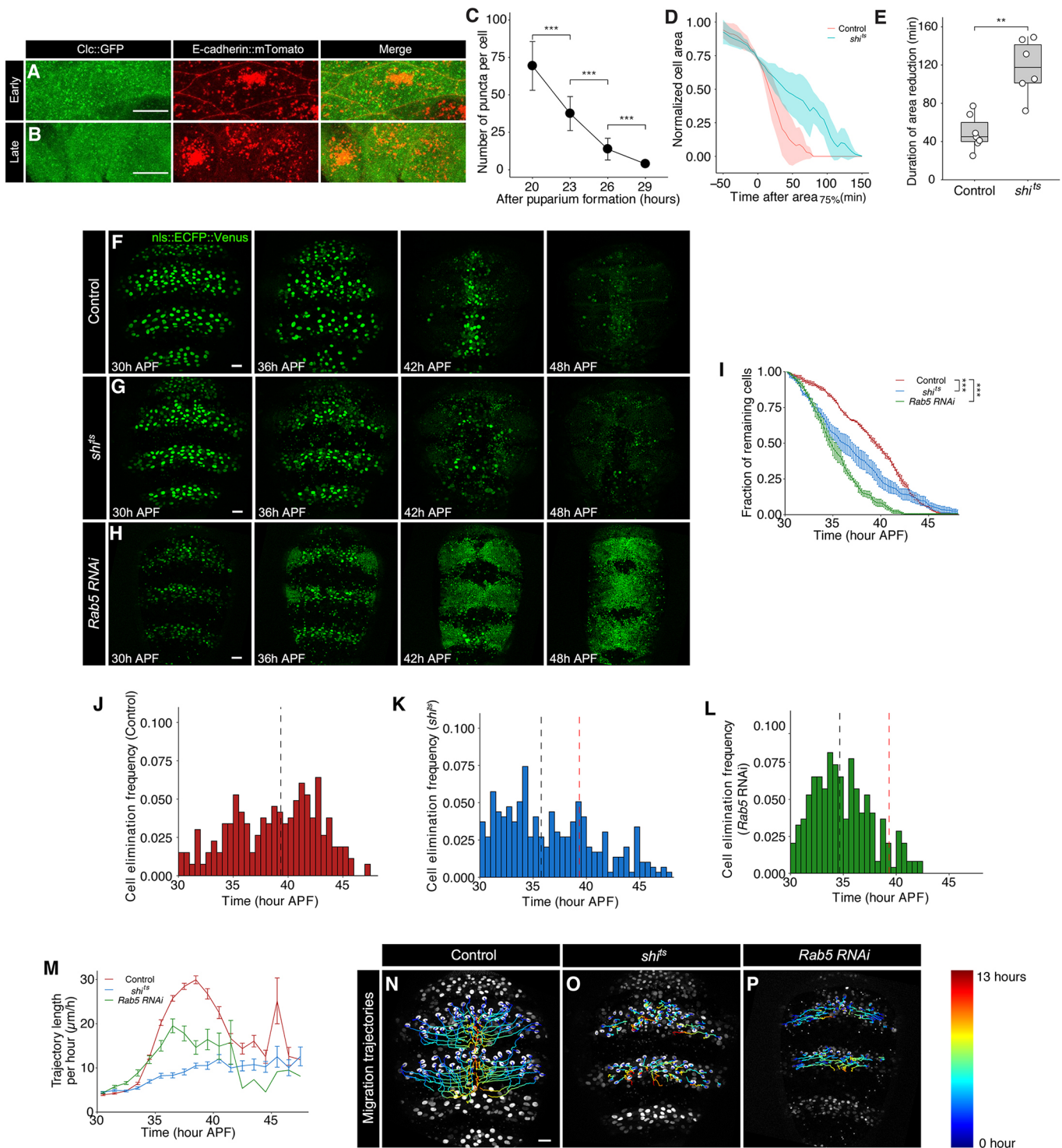


Fig. 2. See next page for legend.

support the hypothesis that the reduction in endocytic activity promotes cell elimination of the LECs.

To assess the effect of reduced endocytic activity on cell elimination further, we took a second genetic approach by manipulating another endocytosis related gene, *Rab5*, which is required for early endosome formation (Bucci et al., 1992; Langemeyer et al., 2018). We found that knockdown of *Rab5* in the LECs produced qualitatively similar results to that of *shi*<sup>ts</sup> (Fig. 2G-I, L, Fig. S1C, Movie 4). These results confirm that reduced endocytic activity stimulates cell elimination of the LECs.

Interestingly, we also found that the inhibition of endocytosis by both *shi*<sup>ts</sup> and *Rab5* RNAi blocked migration of LECs (Fig. 2M-P, Fig. S2C, Movies 3 and 4), suggesting that endocytosis is required in the migration of LECs.

#### Myosin II levels increase in the late stage and accelerate cell elimination

Having established that the reduction of endocytosis promotes the elimination of LECs, we set out to investigate the antagonistic



**Fig. 2. Reduction of endocytic activity causes elimination of LECs.** (A,B) Endocytic activity monitored by clathrin light chain tagged with GFP (Clc::GFP) at the early stage (20 h APF, A) and the late stage (30 h APF, B) from control pupae. Adherens junctions are labeled with endogenous E-cadherin tagged with tdTomato (red) (Huang et al., 2009). Note that fewer Clc::GFP puncta are observed at the late stage. Anterior is up. Scale bars: 10  $\mu\text{m}$ . (C) Quantification of Clc::GFP puncta per cell over time.  $n=3$  pupae, 12 cells. Mann–Whitney  $U$ -test,  $***P<0.001$ . (D) Mean area over time for extruding LECs for RT control (red) and *shi*<sup>ts</sup> (blue) during the early stage. Normalized cell areas are plotted against the time after each cell reaches 75% of its initial cell area. Shaded area represents s.d. (E) Duration of area reduction for extruding LECs during the early and the late stages. Mann–Whitney  $U$ -test,  $**P<0.01$ .  $n=7$  cells, control;  $n=6$  cells, *shi*<sup>ts</sup>. (F–H) Time course of LEC elimination from pupae under the restrictive temperature (raised at 18°C then shifted to 29°C at 6 h before imaging) for RT control (F), *shi*<sup>ts</sup>-expressing (G) and *Rab5* RNAi (H) pupae. Note that the GFP marker signal intensity in the LECs was strongly reduced upon *Rab5* RNAi and therefore the gain level for signal detection was enhanced to the level that low GFP expression in the histoblasts became visible at late stages. Anterior is up. Scale bars: 50  $\mu\text{m}$ . (I) Time course analysis of the fraction of remaining LECs for RT control (red), *shi*<sup>ts</sup>-expressing (blue) and *Rab5* RNAi (green) pupae.  $n=2$  segments of 3 pupae. Error bars are s.e.m. Kolmogorov–Smirnov test,  $***P<0.001$ . (J–L) Histograms of the number of eliminated cells for RT control (J, 265 cells), *shi*<sup>ts</sup>-expressing (K, 296 cells) and *Rab5* RNAi (L, 245 cells) pupae under the restrictive temperature at each time point. Bin size is 0.5 h.  $n=2$  segments of 3 pupae for all experiments. Dashed lines indicate the median value for RT control (red), *shi*<sup>ts</sup> and *Rab5* RNAi (black) LECs. (M) The rate of LEC migration at each time point for RT control (red), *shi*<sup>ts</sup>-expressing (blue) and *Rab5* RNAi (green) pupae.  $n=2$  segments of 3 pupae. Error bars are s.e.m. (N–P) Migration trajectories of LECs for RT control (N), *shi*<sup>ts</sup>-expressing (O) and *Rab5* RNAi (P) pupae under the restrictive temperature. Scale bar: 60  $\mu\text{m}$ .

activity of endocytosis against cell elimination in greater detail. We began by examining Myosin II, a principal regulator of the apical constriction that drives LEC extrusion (Ninov et al., 2007; Teng et al., 2017). In order to analyze the dynamics of Myosin II subcellular localization, we generated a transgenic fly with Myosin II tagged with the fluorescent protein Venus using CRISPR/CAS9-mediated genome editing. The apically constricting LECs in the early stage displayed a strong ring-like accumulation of Myosin II, which remained constant at the apical level throughout the entire process, as previously reported (Fig. S3A) (Teng et al., 2017). Myosin II in the static LECs stably localized at the cell cortex apically (Fig. 3A,A'). In contrast, at the late stage, Myosin II exhibited discontinuous accumulation at the cell cortex more basally with higher intensity than at the early stage (Fig. 3B,B'). Moreover, Myosin II labeling showed the contour of LEC apical regions to be separated from their neighbors, leaving gaps between cells at the late stage, which suggests that cell morphology also dynamically changes (Fig. 3E). This observation is consistent with the idea that the LECs change their properties gradually towards the late stage as their endocytic activity diminishes.

In order to analyze the function of Myosin II in the LECs, we next sought to inhibit Myosin II activity by overexpressing a constitutively active form of the Myosin II phosphatase MBS, which inactivates the Myosin II regulatory light chain by dephosphorylation (Fukata et al., 1998; Lee and Treisman, 2004). Whereas the effect of expression of constitutively active MBS on Myosin II localization in the early LECs was relatively weak, it was severely reduced at the late stage, indicating that the dynamic Myosin II activity observed at the late stage is more sensitive to this genetic treatment (Fig. S3B–D). This result allowed us to test the effect of Myosin II inhibition especially at the late stage. Interestingly, the rate of cell elimination was comparable to the control at the early stage and lower than control at the late stage resulting in a monotonic temporal cell elimination pattern throughout the tissue remodeling process whereby Myosin II is inhibited by the MBS

expression (Fig. 3F–H, Movie 5). These data show that the increased levels and dynamic activity of Myosin II at the late stage contribute to the acceleration of LEC elimination. As the time course of Myosin II localization parallels with the change in the endocytic activity, it is possible that Myosin II levels are regulated by endocytosis.

### Reduced endocytosis activity stimulates the accumulation of Myosin II

The results presented so far indicate that the mechanism of cell elimination at the late stage may be distinct from that of the early stage. Therefore, we next tested whether the distinct localization of Myosin II is the consequence of reduced endocytic activity, which is observed at the late stage of normal development. Inhibition of endocytosis by expressing either *shi*<sup>ts</sup> or *Rab5* RNAi recapitulated the increased junctional Myosin II accumulation (Fig. S4A–E). Moreover, discontinuous accumulation at the cell junction was observed at a more basal level, which is characteristic of the late LECs (Fig. 3C–D', Movies 6–9), indicating that lowering endocytic activity is sufficient to induce the late-stage-type LEC. In addition, area constriction was not accelerated, but rather was slowed down by the reduction of endocytosis (Fig. 2D,E). The speed of LEC area constriction at the late stage upon Myosin II inhibition was also comparable to controls at the late stage (Fig. 3I–L), suggesting that Myosin II does not provide a major driving force for cell extrusion and instead acts to promote cell elimination at a more upstream level at the late stage, unlike at the early stage (Teng et al., 2017). From these results, we conclude that reduced endocytosis regulates Myosin II levels as well as cell elimination without accelerating area constriction. We propose that the increased Myosin II levels triggered by reduced endocytic activity at the late stage contribute to the priming of LECs for elimination from the tissue, thereby accelerating tissue remodeling. Consistent with this idea, inhibition of Myosin II alleviated the hastened cell elimination caused by blocking endocytosis (Fig. 3M–O).

### Reduced endocytic activity induces the reduction of E-cadherin levels

Myosin II exerts a contractile force on cell-cell junctions through the formation of the cortical actomyosin network that both directly and indirectly interacts with adherens junction components, including E-cadherin (Yamada et al., 2005; Desai et al., 2013; Takeichi, 2014; Röper, 2015; Vasquez and Martin, 2016). E-cadherin levels at the adherens junctions of the LECs were reduced as they transitioned to the late stage, despite the increase in Myosin II levels at this stage (Fig. 4A–B, Fig. S3D) (Bischoff, 2012). Consistent with this observation, inhibition of endocytosis by the expression of *shi*<sup>ts</sup> and *Rab5* RNAi reduced junctional E-cadherin levels in the LECs, indicating that E-cadherin at the adherens junctions is positively regulated by endocytosis (Fig. 4C–F). These results suggest that lowering endocytic activity induces the reduction of E-cadherin levels rather than increasing them. This relationship between endocytosis and E-cadherin levels on cell junctions is incompatible with the well-established role of endocytosis in promoting internalization/turnover of E-cadherin in the embryonic epidermis, the notum and the wing epithelium during the pupal development in *Drosophila* (Georgiou et al., 2008; Levayer et al., 2011; Jewett et al., 2017; Iyer et al., 2019). Our data implies that the reduced endocytic activity does not result in junctional E-cadherin accumulation but instead lowers junctional E-cadherin via an unknown mechanism in the LECs during tissue remodeling. Interestingly, fluorescence recovery after photobleaching (FRAP) assays revealed that blocking endocytosis reduces both the mobile fraction and the turnover rate of E-cadherin, suggesting that endocytosis promotes internalization of E-cadherin as observed in

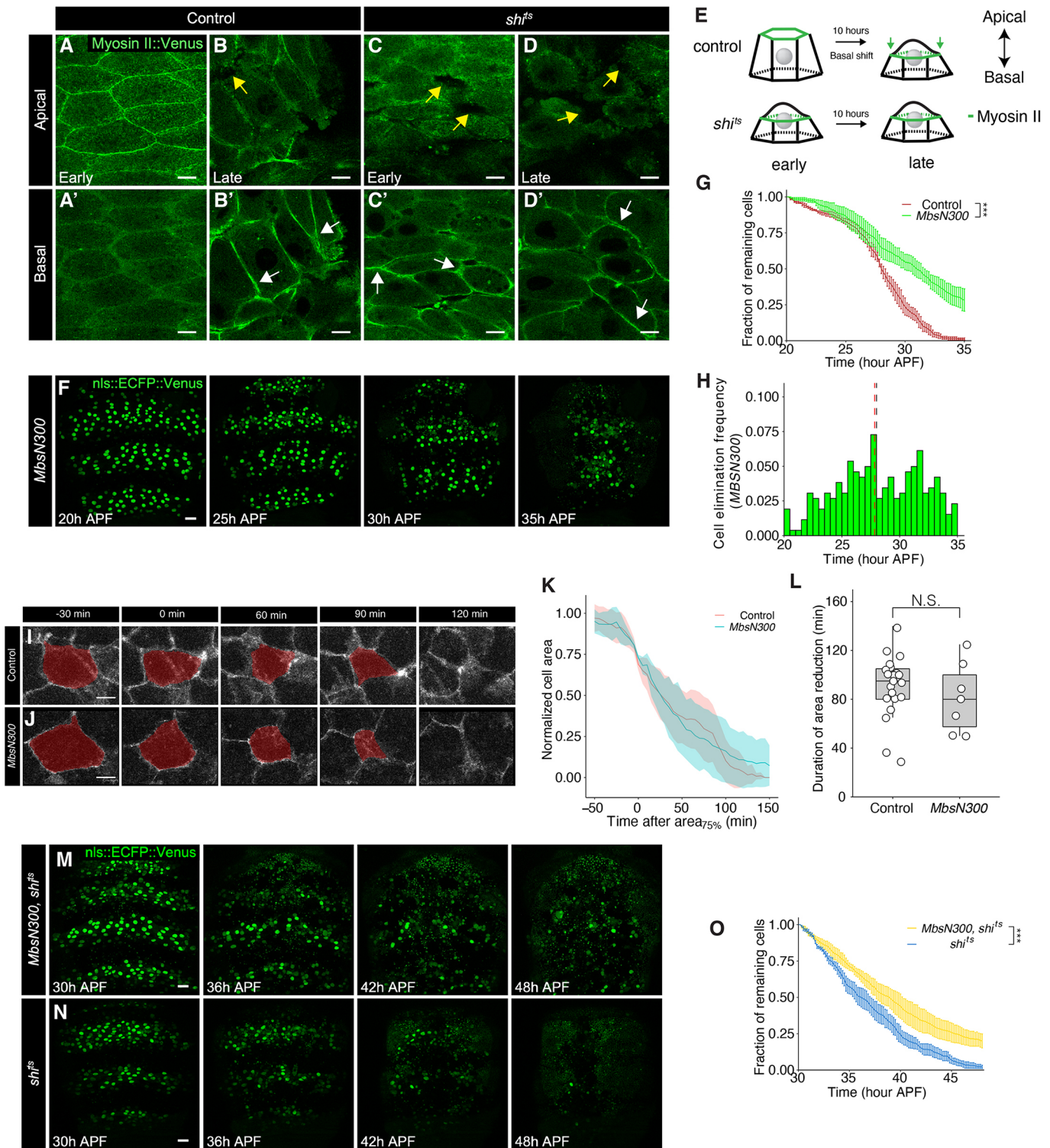


Fig. 3. See next page for legend.

other tissues (Fig. S5A). We therefore hypothesized that there is an additional mode beyond the internalization of E-cadherin that regulates junctional E-cadherin downstream of endocytosis.

#### Cell elimination induced by reduced endocytic activity absolutely requires caspase activation

Cell elimination during epidermal remodeling has been shown to be dependent on caspase activation (Ninov et al., 2007). To monitor

caspase activation directly, we used a fluorescence resonance energy transfer (FRET)-based active caspase indicator, nucleus-localized SCAT3, to visualize the effector caspase protease activity live (Takemoto et al., 2003; Koto et al., 2009). We observed caspase activation up to 5 min before cell elimination as judged by nuclear fragmentation in both RT control and *shi<sup>ts</sup>* experiments (Fig. 5A,B, Fig. S6A, Movies 10 and 11). The time course of the FRET ratio revealed similar temporal patterns to that of cell elimination in both



**Fig. 3. Myosin II reorganizes and is required for the acceleration of LEC elimination.** (A-D') Subcellular localization of myosin II tagged with Venus (MyoII::Venus) in RT control (A-B') and *shi<sup>ts</sup>*-expressing (C-D') pupae at the early (A,A',C,C') and late stage (B,B',D,D') in apical (A-D) and basal (2-3  $\mu$ m below the apical section) cross-sections (A'-D'). White and yellow arrows indicate thick cortical accumulation and gaps between cells, respectively. Images were taken from live pupae. Anterior is up. Scale bars: 10  $\mu$ m. (E) Schematic of the Myosin II distribution for RT control and *shi<sup>ts</sup>* LECs at the early and late stages. (F) Time course of LEC elimination in pupa expressing the Myosin phosphatase catalytic domain *MbsN300* at 25°C. Anterior is up. Scale bar: 50  $\mu$ m. (G) Time course analysis of the fraction of remaining LECs for control (red) and *MbsN300*-expressing (green) pupae. Error bars are s.e.m.  $n=3$  pupae. Kolmogorov–Smirnov test, \*\*\* $P<0.001$ . (H) Histogram of the number of eliminated cells for *MbsN300*-expressing pupae. Bin size is 0.5 h.  $n=2$  segments of 3 pupae, 261 cells. Dashed lines indicate the median value for control (red) and *MbsN300*-expressing (black) LECs. (I,J) Images of area reduction for extruding LECs for control (I) and *MbsN300*-expressing (J) pupae labeled with an Nrg-GFP protein trap line. Scale bars: 10  $\mu$ m. (K) Mean area over time for extruding LECs for control (red) and *MbsN300*-expressing (blue) pupae during the late stage. Normalized cell areas are plotted against the time after each cell reaches 75% of its initial cell area. Shaded area represents s.d. (L) Duration of area reduction for extruding control and *MbsN300*-expressing LECs during the late stages. Mann–Whitney *U*-test. N.S., not significant.  $n=21$  cells, control;  $n=10$  cells, *MbsN300* overexpression. (M,N) Time course of LEC elimination in pupa expressing *MbsN300* and *shi<sup>ts</sup>* at 29°C (M), in comparison with LECs expressing *shi<sup>ts</sup>* alone (N). Anterior is up. Scale bars: 50  $\mu$ m. (O) Time course analysis of the fraction of remaining LECs expressing *MbsN300* and *shi<sup>ts</sup>*, versus those expressing *shi<sup>ts</sup>* alone (yellow) pupae. Error bars are s.e.m.  $n=3$  pupae. Kolmogorov–Smirnov test, \*\*\* $P<0.001$ .

RT control and endocytosis inhibition by *shi<sup>ts</sup>* conditions, suggesting that LECs with defective endocytic activity undergo apoptotic cell death just like normal cells (Fig. 5C,D, Fig. S6A). Given that the inhibition of endocytic activity affects the E-cadherin level rather uniformly in the entire region, it is possible that caspase activation may occur at a weaker level that is non-apoptotic in a tissue-wide manner to prime cells for elimination. Using a more sensitive reporter, Apoliner (Bardet et al., 2008; Levayer et al., 2016), we revealed that caspase activity was uniformly upregulated during the late stage (Fig. 5E, 40 h APF). Moreover, caspase activity was upregulated already at an earlier stage in *shi<sup>ts</sup>*, suggesting that the reduction in endocytic activity stimulates a weak level of caspase activation (Fig. 5F, 34 h APF). We next asked whether the cell elimination induced by the inhibition of endocytosis is dependent on caspase activation. Overexpression of the caspase inhibitor *Diap1* in the LECs suppressed cell elimination (Fig. 5G,I). The migration of LECs was not blocked by *DIAP1* overexpression, suggesting that cell migration is not a mere consequence of massive cell elimination (Fig. S6B-E). Strikingly, the expression of *Diap1* completely blocked cell elimination induced by the inhibition of endocytosis (Fig. 5H,I, Movie 12). These results suggest that reduced endocytic activity signals the caspase activation pathway initially to a non-apoptotic level, then eventually to the level that triggers cell elimination, and that cell elimination induced by the reduced endocytosis absolutely requires caspase activation.

### E-cadherin exhibits antagonistic mutual repression with caspase activation, but Myosin II upregulation is independent of caspase activation

So far, our results indicate that reduced endocytic activity in the LECs induces upregulation of Myosin II dynamics, downregulation of E-cadherin levels, and activation of caspases. Next, we investigated how the changes in Myosin II and E-cadherin levels are related to caspase activation in the LECs. Active caspases have been shown to proteolytically degrade the adherens junction components E-

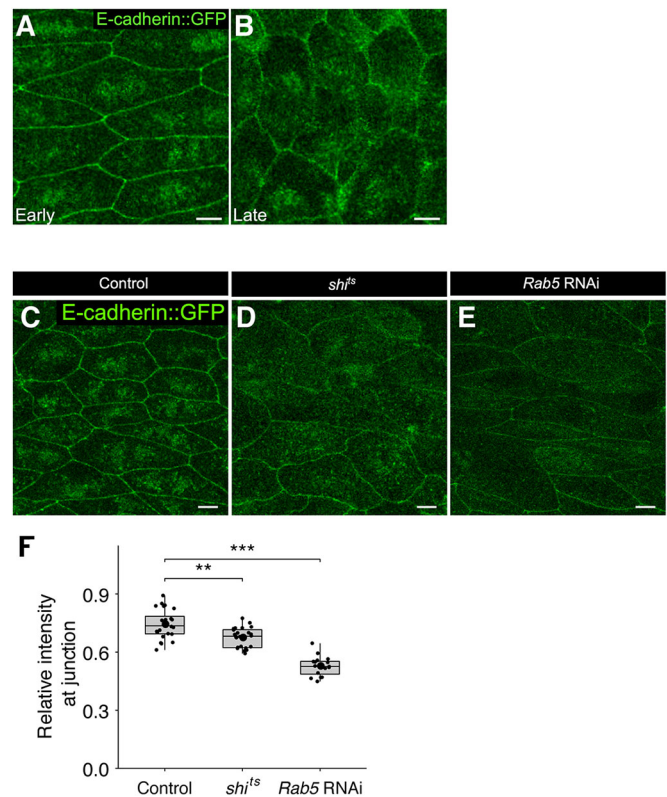


**Fig. 4. Reduced endocytic activity reduces E-cadherin levels.** (A,B) E-cadherin localization visualized by E-cadherin::GFP at the early (20 h APF at 25°C) and late (30 h APF at 25°C) stages for control pupa. Images were generated by maximum intensity projection. Scale bars: 10  $\mu$ m. (C-E) E-cadherin localization at the early stage for RT control (C), *shi<sup>ts</sup>*-expressing (D) and *Rab5* RNAi (E) pupae. Images were generated by maximum intensity projection. Anterior is up. Scale bars: 10  $\mu$ m. (F) Quantification of signal intensity of junctional E-cadherin::GFP in RT control, *shi<sup>ts</sup>*-expressing and *Rab5* RNAi LECs relative to the control region in each pupa. One-way ANOVA followed by post-hoc Tukey test, \*\* $P<0.01$ , \*\*\* $P<0.001$ .  $n=2$  pupae, >18 cells each.

cadherin in mammalian cells and  $\beta$ -catenin in both mammalian cells and *Drosophila* embryos (Brancolini et al., 1997; Bannerman et al., 1998; Steinhilber et al., 2001; Chandraratna et al., 2007; Kessler and Müller, 2009). Accordingly, we found that overexpression of *Diap1* increased E-cadherin on cell junctions of the LECs at the late stage (Fig. 6A-B'). In contrast, we observed no increase of E-cadherin upon overexpression of *Diap1* at the early stage, suggesting that overexpression of *Diap1* does not increase the basal level of junctional E-cadherin but instead suppresses the effect of the developmentally controlled reduction of the E-cadherin levels (Fig. 6A-B'). Similarly, the reduced E-cadherin levels induced by the endocytosis inhibition were recovered when caspase was simultaneously inhibited, suggesting that caspase activation is required for lowering E-cadherin levels induced by the reduction of endocytosis (Fig. 6C-E). Reduction of E-cadherin levels by RNAi promoted the elimination of LECs (Fig. 6F,H,I, Fig. S7A, Movie 13). Interestingly, the acceleration of cell elimination induced by the reduction of E-cadherin was alleviated by *Diap1* overexpression (Fig. 6G,H, Movie 14). This result suggests that the elimination of LECs caused by reducing the E-cadherin levels also requires caspase activity despite the fact that the E-cadherin level was regulated by caspase activation when endocytosis was blocked. Altogether, our results provide genetic evidence that the mutual suppression between



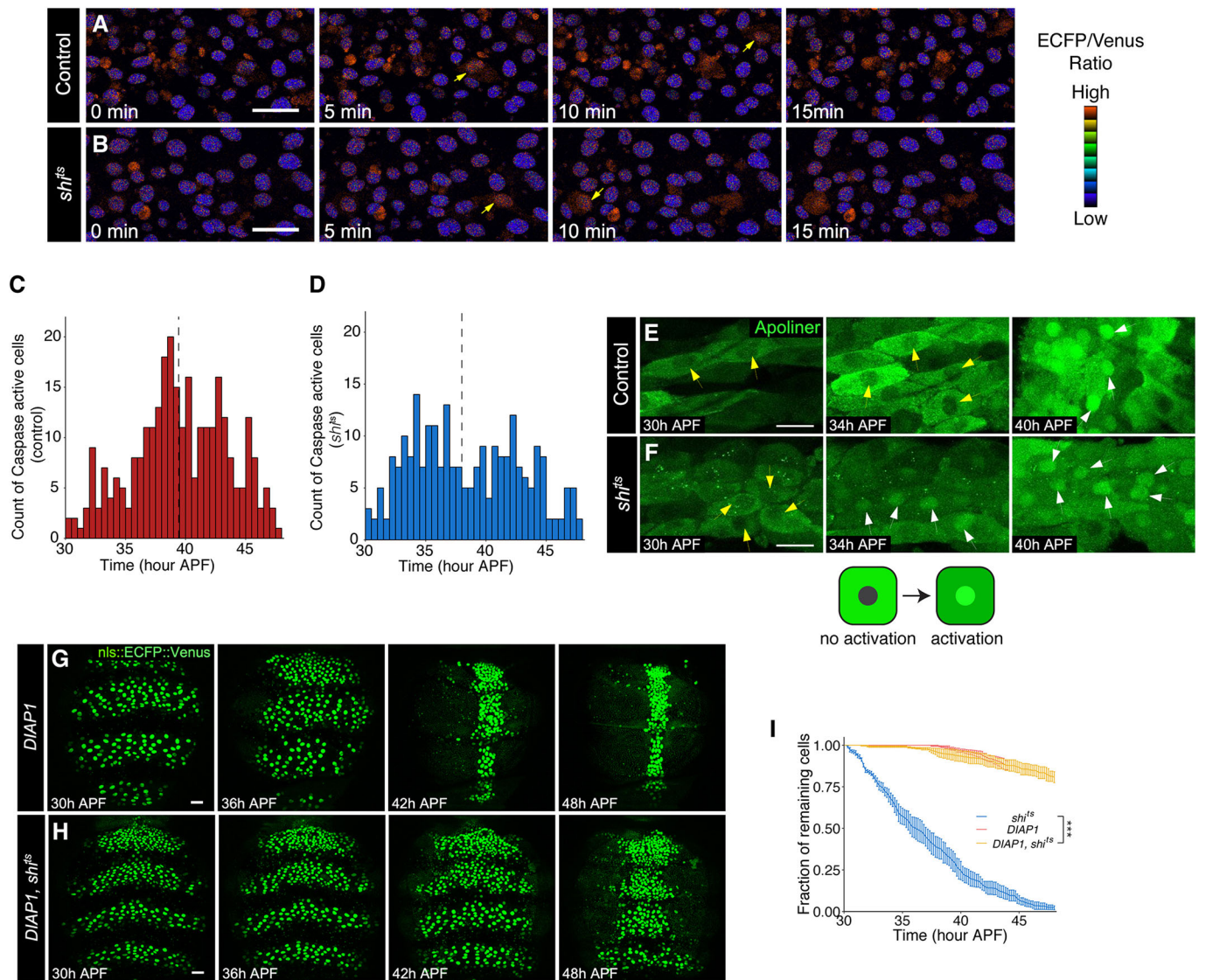


**Fig. 5. Cell elimination caused by reduced endocytic activity is dependent on caspase activation.** (A,B) Time course of the FRET ratio of the nuclear-localized SCAT3 caspase activation indicator (ECFP/Venus) for RT control (A) and *shi<sup>1s</sup>*-expressing (B) LECs. The higher FRET ratio indicates higher caspase activity. Yellow arrows indicate high FRET ratio LECs. Anterior is up. Scale bars: 50  $\mu$ m. (C,D) Histogram of the number of the SCAT3 FRET-positive cells for RT control (C) and *shi<sup>1s</sup>*-expressing (D) LECs. Bin size is 0.5 h.  $n=2$  segments of 3 pupae, 295 cells for RT control and 242 cells for *shi<sup>1s</sup>* expressing LECs. Dashed lines indicate the median value for RT control and *shi<sup>1s</sup>*-expressing LECs. (E,F) Caspase activation probed by the Apoliner reporter at different time points for control (E) and *shi<sup>1s</sup>*-expressing (F) LECs. Cells with high caspase activity are labeled with nuclear localized GFP signal (white arrows). Cells with low caspase activity are labeled with yellow arrows. Representative data from  $n=3$  pupae at each time point. Anterior is up. Scale bars: 40  $\mu$ m. (G,H) Time course of LEC elimination from pupae under the restrictive temperature for *Diap1*-expressing (G) and *Diap1*- and *shi<sup>1s</sup>*-expressing (H) pupae. Anterior is up. Scale bars: 50  $\mu$ m. (I) Time course analysis of the fraction of remaining LECs for *shi<sup>1s</sup>*-expressing (blue), *Diap1*-expressing (red), and *Diap1*- and *shi<sup>1s</sup>*-expressing (orange) pupae. Error bars are s.e.m.  $n=3$  pupae for each experiment. Kolmogorov–Smirnov test, \*\*\* $P<0.001$ .

caspases and junctional E-cadherin forms a positive-feedback loop that enables rapid caspase activation at the late stage when the cell elimination process is initiated by the reduction of endocytic activity. Concordantly, increased cell elimination rate induced by the reduced endocytic activity was moderately suppressed at the late stage by supplying additional E-cadherin (Fig. 6J–L, Movie 15). In contrast to E-cadherin, Myosin II levels were upregulated at the early stage when endocytosis is blocked, as well as at the late stage of the normal pupal development (Fig. 3A–D). This upregulation caused by the inhibition of endocytosis was not suppressed by the *Diap1* overexpression, suggesting that the increase in Myosin II is independent of caspase activity, unlike that of E-cadherin (Fig. S7B). Therefore, Myosin II acts upstream of or in parallel with the caspase activation. Together,

our data indicate that reduced endocytosis causes E-cadherin downregulation and Myosin II upregulation in a caspase activation-dependent and -independent manner, respectively, and that both pathways contribute to the acceleration of LEC elimination in the late stage of tissue remodeling.

#### Endosomal trafficking to lysosomes is required for preventing hastened cell elimination

Lastly, we addressed whether cell elimination caused by reduced endocytosis is regulated by the degradation pathway. Trafficking of endosomal vesicles to the lysosomal degradation pathway requires the small GTPase Rab7 (Vanlandingham and Ceresa, 2009; Langemeyer et al., 2018). Knockdown of *Rab7* by RNAi

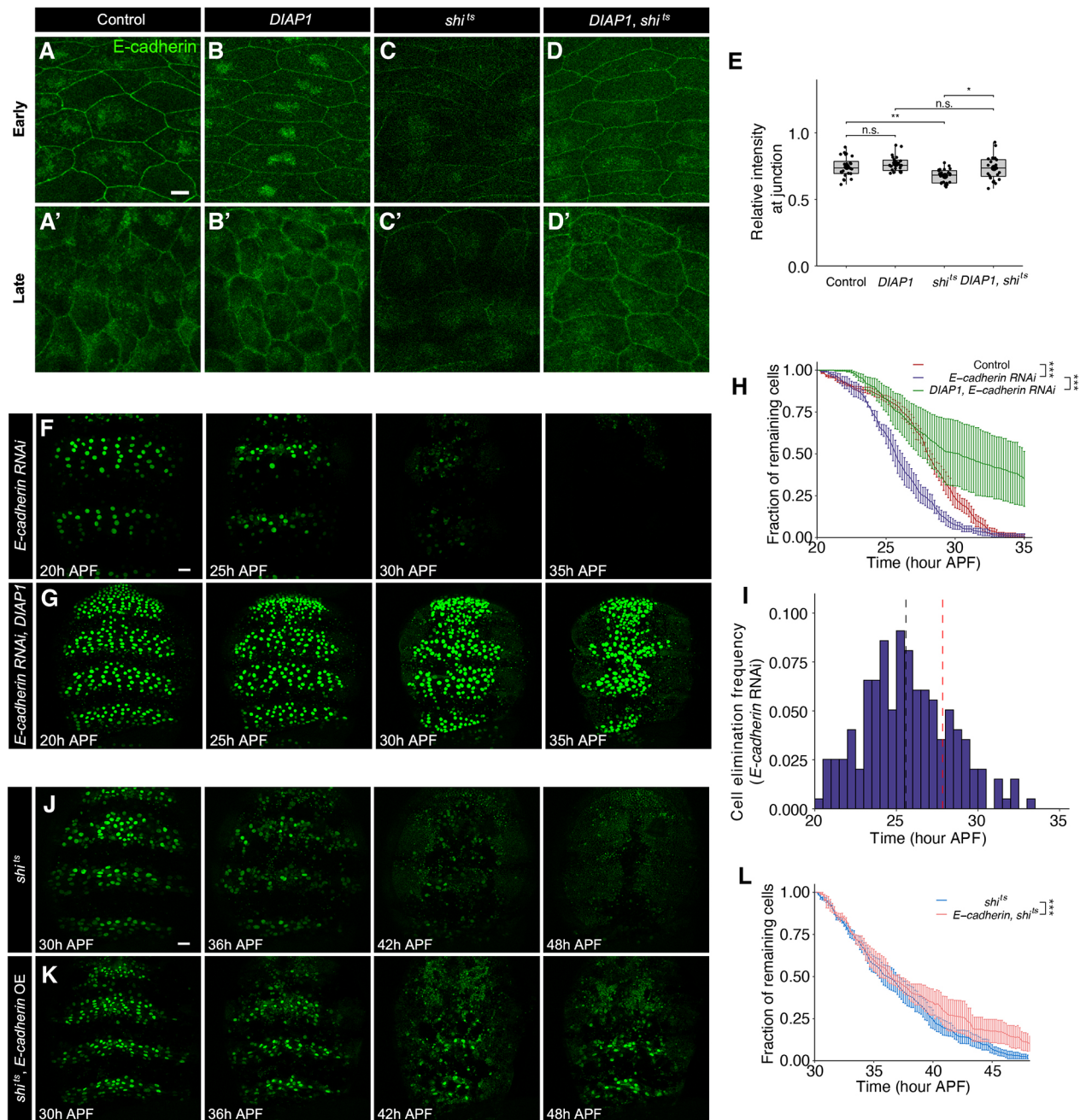


**Fig. 6. Junctional E-cadherin is downregulated by the reduction of endocytic activity in a caspase activation-dependent manner.** (A-D') E-cadherin localization at the early stage (A-D) and the late stage (A'-D') at 25°C for control (A,A') and under the restrictive temperature for *Diap1*-expressing (B,B'), *shi<sup>ts</sup>*-expressing (C,C'), and *Diap1*- and *shi<sup>ts</sup>*-expressing (D,D') pupae. Anterior is up. Scale bar: 10  $\mu$ m. (E) Quantification of signal intensity of junctional E-cadherin::GFP in RT control, *Diap1*-expressing, *shi<sup>ts</sup>*-expressing, and *Diap1*- and *shi<sup>ts</sup>*-expressing LECs relative to the control region in each pupa at the early stage. One-way ANOVA followed by post-hoc Tukey test, \* $P < 0.05$ , \*\* $P < 0.01$ . n.s., not significant.  $n = 3$  pupae, 27 cells each. (F,G) Time course of LEC elimination for *E-cadherin* RNAi (F) and *E-cadherin* RNAi and *Diap1*-overexpressing (G) LECs at 25°C. Anterior is up. Scale bar: 50  $\mu$ m. (H) Time course analysis of the fraction of remaining LECs for *E-cadherin* RNAi, and *E-cadherin* RNAi and *Diap1*-overexpressing pupae at 25°C. Error bars are s.e.m. Kolmogorov–Smirnov test, \*\*\* $P < 0.001$ .  $n = 3$  pupae each. (I) Histogram of the number of eliminated cells for *E-cadherin* RNAi pupae. Bin size is 0.5 h.  $n = 2$  segments of 3 pupae, 198 cells. Dashed lines indicate the median value for control (red) and *E-cadherin* RNAi (black) LECs. (J,K) Time course of LEC elimination under the restrictive temperature for *shi<sup>ts</sup>*-expressing (J) and *shi<sup>ts</sup>*- and *E-cadherin*-overexpressing (K) LECs. Anterior is up. Scale bar: 50  $\mu$ m. (L) Time course analysis of the fraction of remaining LECs for *shi<sup>ts</sup>*-expressing, and *shi<sup>ts</sup>*-expressing and *E-cadherin*-overexpressing LECs under the restrictive temperature. Error bars are s.e.m. Kolmogorov–Smirnov test, \*\*\* $P < 0.001$ .  $n = 3$  pupae each.

promoted the elimination of LECs, similar to *shi<sup>ts</sup>* and *Rab5* RNAi (Fig. 7A-C, Fig. S8A,B, Movie 16). Similarly, E-cadherin levels were reduced and the upregulation of Myosin II levels was observed upon RNAi of *Rab7* (Fig. 7D-I). Knockdown of *Rab7* essentially recapitulated all the features that were observed in the reduction of

endocytic activity. Therefore, we conclude that endosomal trafficking to lysosomes is crucial for preventing the LEC elimination that is induced by the reduction of endocytosis. We cannot rule out the possibility that the recycling pathway may also be at work in parallel, which would antagonize the acceleration of



cell elimination in the late stage through the stabilization of junctional E-cadherin. Altogether, our results suggest that the endocytic pathway, including trafficking to lysosomes, is required for preventing hastened cell elimination and for the developmentally programmed reduction of endocytosis that primes the LECs to undergo rapid cell elimination in the late stage of tissue remodeling.

## DISCUSSION

We investigated the developmental control mechanism that accelerates massive cell elimination during the remodeling of epidermal tissue in the pupal *Drosophila* abdomen. During tissue remodeling, large LECs are replaced by rapidly proliferating histoblasts, with the entire process completing within a mere 20 h. Until now, the mechanism that regulates rapid cell elimination during this process has been unknown. Here, we found that the endocytic activity of the LECs attenuates as tissue remodeling progresses. The reduction of endocytic activity correlates with increased cell elimination frequency and is sufficient to trigger the acceleration of cell elimination by changing cellular physiological properties. The acceleration of cell elimination requires an increase in Myosin II activity and caspase activation. Moreover, caspase activation involves a positive-feedback loop with the reduction of E-cadherin levels resulting from their mutual suppression. This positive feedback would help raise a non-apoptotic level of caspase activation to an apoptotic level. We propose that the change in endocytic activity serves as a switch to trigger the transition of the physiological properties of the LECs, which facilitates tissue remodeling by accelerating the cell elimination rate.

### Change in endocytic activity switches physiological cell properties

Our study identified the previously unknown mechanisms involved in the developmental transition of endocytic activity that regulates cell elimination. Endocytosis plays a role in the regulation of numerous cellular activities, including cell proliferation, differentiation and metabolism through endosomal trafficking of transmembrane proteins (Sigismund et al., 2012). In animal development, endocytosis functions in the formation of morphogen gradients and modulation of the activity of receptor proteins in some signal transduction pathways (Seto et al., 2002; Fischer et al., 2006). We used live imaging to show that the endocytic activity of the LECs gradually attenuates over the course of tissue remodeling. The reduction of endocytic activity was accompanied by reduced migration activity and increased cell elimination together with the upregulation of Myosin II and the downregulation of E-cadherin. Our genetics experiments suggest that those physiological changes are caused by the reduction of the endocytic activity. There are several reports that indicate that Myosin II is regulated by signal transduction pathways that are positively or negatively regulated by the endocytosis. Myosin II activity is, for example, regulated by several signaling receptors, including G-protein coupled receptors (GPCRs), tumor necrosis factor  $\alpha$  (TNF $\alpha$ ) and epidermal growth factor receptor (EGFR) (Goetzl and An, 1998; Malliri et al., 1998; Kjølner and Hall, 1999; Puls et al., 1999; Rossman et al., 2005). It is plausible that endocytosis regulates Myosin II subcellular localization patterns and dynamics by trafficking some signaling receptors during LEC elimination. Endocytosis is known to regulate cell migration through the internalization and trafficking of the adhesion molecule integrins (Palecek et al., 1996; Kamiguchi and Lemmon, 2000). Moreover, blocking endocytosis leads to the

activation of the death receptors TRAIL-R1 and TRAIL-R2 in cancer cell lines (Austin et al., 2006; Zhang and Zhang, 2008). Although it is known that the *Drosophila* TNF pathway is upregulated by endocytosis (Igaki et al., 2009), no endocytosis-inactivated death receptor has been identified in *Drosophila* thus far. Recent work showed that the *Drosophila* caspase-3, DrICE, shows spatial subcellular localization to confer non-apoptotic functions (Amcheslavsky et al., 2018; McSharry and Beitel, 2019). DrICE is associated with endosomes and regulates trafficking of proteins in tracheal development (McSharry and Beitel, 2019). Our results suggest another aspect of the link between trafficking and caspase activation. It will be interesting to determine the dynamics of subcellular localization of caspases during the tissue remodeling process to understand the mechanism regulating caspase activity.

### Myosin II plays multiple roles in LEC elimination

Previous work has found that cortical Myosin II localization is regulated by caspase activation in LECs (Teng et al., 2017). We found that cortical localization of Myosin II becomes independent in the late stage of development. In the early stage, Myosin II dynamically accumulates in a ring-like structure at the cortex only in apically constricting cells. The formation of this constricting ring requires caspase activity (Teng et al., 2017). Whereas the early LECs form the dense cortical ring in a caspase activity-dependent manner, the late Myosin II dynamics and their discontinuous cortical accumulation do not depend on caspase activity. Notably, both the regulating molecular mechanisms and the physiological roles of the distinct Myosin II dynamics differ by mode: the caspase-dependent Myosin II accumulation acts only transiently when the LECs undergo apical constriction-driven cell elimination whereas the Myosin II reorganization induced by decreased endocytosis, by contrast, is observed all over the tissue.

Importantly, at both stages Myosin II promotes cell elimination, but how it acts may differ. We propose that Myosin II in early and late LECs operates at different hierarchical layers. Whereas the early stage Myosin II mainly contributes to the execution of apical constriction-driven cell elimination by exerting contractile forces on the cell junctions, the late stage Myosin II does not contribute to the area reduction but rather contributes to increasing the potential of cell death. One of the possible molecular targets that the increased Myosin II activity potentiates would be caspases. Myosin II may act upstream of caspase activation because the increase in Myosin II activity is not altered upon caspase inhibition. In support of this idea, it is reported that programmed cell death and caspase activation are dependent on Rho-associated protein kinase (ROCK) activity, which activates Myosin II, in several cell types (Petrache et al., 2001, 2003; Minambres, 2006; Okumura et al., 2016). Therefore, it is tempting to speculate that Myosin II potentiates caspase activity in the LECs, either directly or indirectly. The effect of Myosin II on caspase activation may involve a biochemical interaction between molecules, but it is also possible that the contractility generated by enhanced Myosin II activity is responsible for regulating caspase activity. The cells adjacent to a faster growing cell population are compressed and often eventually eliminated by apoptosis (Levayer et al., 2016; Brás-Pereira and Moreno, 2018). A recent report showed that this process involves mechanical sensing of cells whereby the compressed cells downregulate EGFR signaling, which is required for cell survival by suppressing caspase activation (Moreno et al., 2019). Whether or not the same mechanoresponsive system operates in tissue remodeling and other systems would be an interesting topic for future investigation.



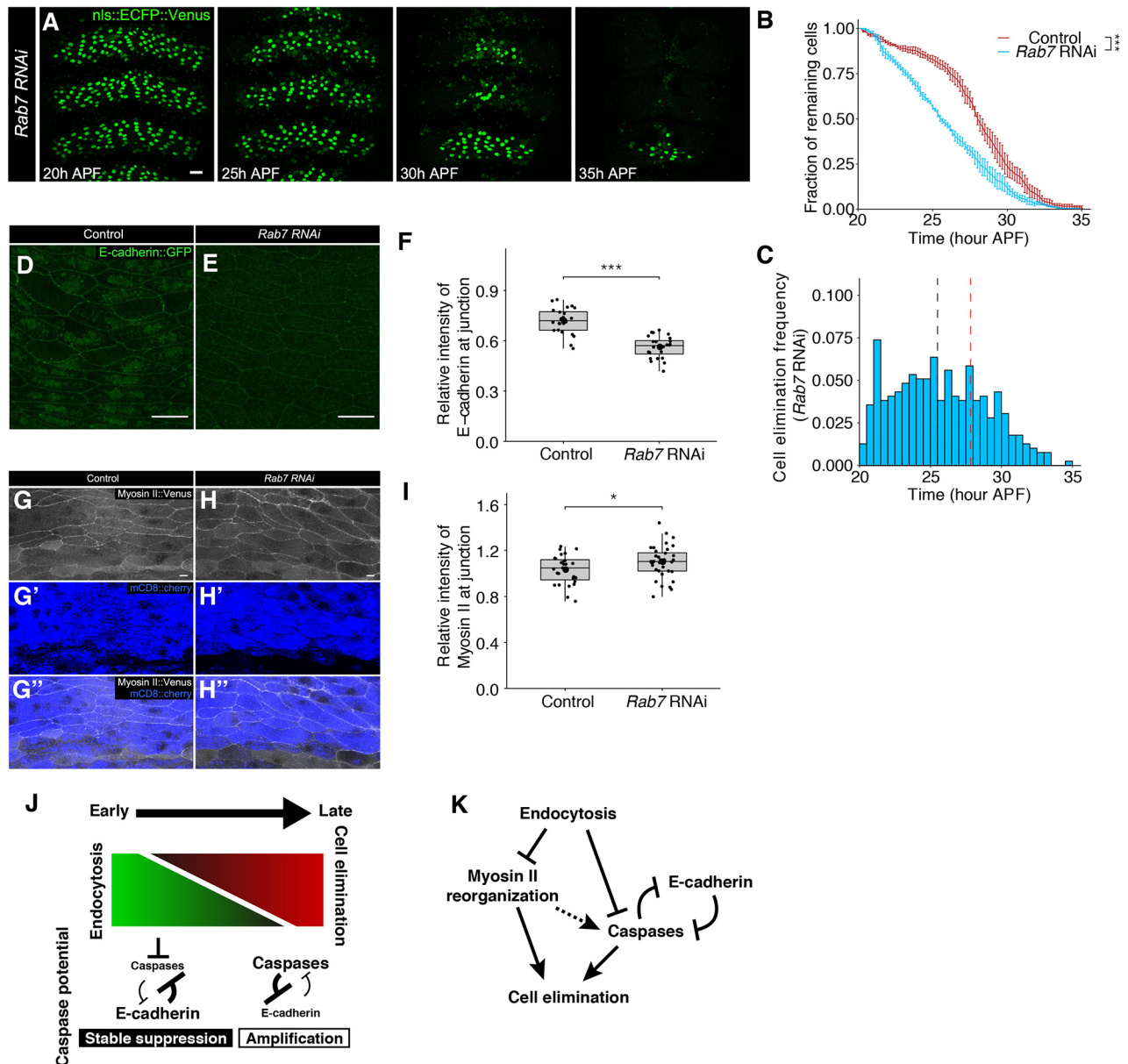


**Fig. 7. Reduced Rab7 phenocopies the accelerated LEC elimination upon blocking endocytosis.** (A) Time course of the LEC elimination for *Rab7* RNAi LECs at 25°C. Anterior is up. Scale bar: 50  $\mu$ m. (B) Time course analysis of the fraction of remaining LECs for *Rab7* RNAi pupae at 25°C. Error bars are s.e.m. Kolmogorov–Smirnov test, \*\*\* $P$ <0.001.  $n$ =3 pupae each. (C) Histogram of the number of eliminated cells for *Rab7* RNAi pupae. Bin size is 0.5 h.  $n$ =2 segments of 3 pupae, 393 cells. Dashed lines indicate the median value for control (red) and *Rab7* RNAi (black) LECs. (D,E) E-cadherin localization at the early stage at 25°C for control (D) and *Rab7* RNAi (E) pupae. Anterior is up. Scale bars: 10  $\mu$ m. (F) Quantification of signal intensity of junctional E-cadherin::GFP in control and *Rab7* RNAi LECs relative to the control region in each pupa. Student's  $t$ -test, \*\*\* $P$ <0.001.  $n$ =3 pupae, 27 cells each. (G-H') Subcellular localization of MyoII::Venus in control (G-G') and *Rab7* RNAi (H-H') LECs. Marker expression (mCD8::cherry) indicates the region of GAL4 expression (G',G'',H',H''). Anterior is up. Scale bars: 10  $\mu$ m. (I) Quantification of signal intensity of MyoII::Venus in the control and *Rab7* RNAi LECs relative to the control region in each pupa for junctional localization. Student's  $t$ -test, \* $P$ <0.05.  $n$ =3 pupae, >27 cells each. (J) Scheme for endocytic activity (green) and cell elimination potential (red) in the LEC during tissue remodeling. LECs at the early stage have high endocytic activity, which represses caspase activity. Low caspase potential is maintained at a stable level by the presence of junctional E-cadherin. At the late stage, developmentally programmed reduction of endocytic activity increases caspase activity. This activation leads to the reduction of E-cadherin, which then further increases the caspase activation potential. (K) Proposed interactions from endocytosis to cell elimination.

### The positive-feedback loop formed between activated caspases and reduced E-cadherin levels amplifies caspase activation

It is well established that endocytosis upregulates E-cadherin turnover by promoting its internalization (Georgiou et al., 2008; Levayer et al., 2011; Iyer et al., 2019). It was initially puzzling that E-cadherin levels decreased with reduced endocytic activity in the

LECs. However, this outcome could be explained by the existence of a parallel pathway that independently regulates E-cadherin levels inversely to the way they are controlled for by endocytosis. Concordant with this hypothesis, E-cadherin levels, which were reduced by blocking endocytosis, recovered when caspase activity was inhibited. This effect was tissue wide and is therefore consistent with the finding that caspase activity was elevated to a non-

apoptotic level across the entire tissue in the endocytosis-defective tissue at an early stage. Therefore, endocytosis can regulate the size of the E-cadherin pool available at adherens junctions through the regulation of caspase activity. Cell elimination induced by reducing E-cadherin levels was also dependent on caspase activation, which suggests the presence of a mutually repressive relationship between E-cadherin and caspase activation. At the early stage, E-cadherin levels are kept high, and therefore caspase activation potential is kept low (Fig. 7J). Conversely, at the late stage, E-cadherin levels are reduced through the caspase activation, which is induced by the attenuation of endocytic activity of the LECs (Fig. 7J). The caspase activation would be initially moderate and not apoptotic. However, owing to the lack of caspase inhibition by repressive E-cadherin, more and more caspases would be activated. This positive-feedback loop amplifies the caspase activation so that it reaches the threshold for apoptosis. It should be noted that it is also possible that a reduced E-cadherin level lowers the threshold of caspase activation. In any case, this positive-feedback system, possibly in parallel or in tandem with the Myosin II pathway, would contribute to the acceleration of cell elimination (Fig. 7K). The existence of this positive-feedback system would explain why the gradual change in endocytic activity can trigger a rapid phase switch in the cell elimination rate. Looking ahead, it will be interesting to understand what determines the order in which different cells die. We assume that there is another factor that triggers cell elimination at the late stage, but it is entirely possible that that elimination could be a consequence of stochastically introduced biochemical or mechanical imbalance between neighbors through the fluctuating cell-cell interactions (Saw et al., 2017).

We found that the interactive network of Myosin II, E-cadherin and caspase activation modulates as tissue remodeling progresses. However, these intricate interactions seem to be regulated in a self-organized manner initiated by the simple, gradual transition of endocytic activity. Given the possibility that the activation of caspase is dependent on sequestration or degradation, the potential cargo of endocytic vesicles would likely be a death receptor, which would induce programmed cell death unless degraded. Identifying the molecular target of endosomal trafficking to lysosomes in this system could provide insights into the rapid turnover of the cells during tissue remodeling. In summary, our work developed a new approach for elucidating the mechanisms potentially common to tissue remodeling in other animal species.

## MATERIALS AND METHODS

### Fly stocks

The following fly strains were used: *sqh::Venus* (this work), *UAS-nls::SCAT3 (UAS-nls::ECFP::Venus)* (Kanuka et al., 2005), *lexAop-nls::SCAT3 (lexAop-nls::ECFP::Venus)* (Nakajima et al., 2011), *pnr-Gal4* (Calleja et al., 1996), *UAS-shi<sup>ts</sup>* (Kitamoto, 2001), *E-cadherin::GFP* (Huang et al., 2009), *UAS-MbsN300* (Lee and Treisman, 2004), *Yrab7* (Dunst et al., 2015), *tubP-LexA::GAD* (Lai and Lee, 2006), *UAS-shg RNAi* (NIG-FLY Stock Center 3722R-1), *UAS-Clc::GFP* (Bloomington Stock Center 7109), *UAS-Rab5 RNAi* (Bloomington Stock Center 34832), *UAS-Rab7 RNAi* (Bloomington Stock Center 27051), *UAS-mCD8::cherry* (Bloomington Stock Center 27392), *UAS-myc::DIAP1* (Hay et al., 1995).

### Generation of transgenic fly by CRISPR/Cas9-based genome editing

To construct a guide RNA (gRNA) vector for generating knock-in for Myosin II::Venus, *spaghetti squash* (*sqh*)-specific oligonucleotides (5'-CTTCGTT-CTGCTCATCCTTGTCCT-3' and 5'-AAACAGGACAAGGATGAGCA-GTAAC-3') were annealed and introduced into U6-gRNA to generate the U6-*sqh*-gRNA vector (Kondo and Ueda, 2013). To generate the homologous

arms for the Myosin II::Venus knock-in construct, the following primers (5'-GCTTGATATCGAATTCATCAGGCGCAGATTGCC-3' and 5'-AGTTG-GGGGCGTAGGCTGCTATCCTTGTCCTTGGC-3' for 5' flanking arm, and 5'-TAGTATAGGAACCTCATCGCCAGCAGTCGATTACTAGC-3' and 5'-CGGGCTGCAGGAATCCCGAAATCTCTTTCAATTTCCCGC-C-3' for 3' flanking arm) were used to amplify the 0.51 kb and 0.55 kb genomic DNA regions flanking the stop codon of the *sqh* gene, respectively. The knock-in cassette containing the Venus-coding sequence was excised from pPVxRF3 (a gift from Dr Shu Kondo, National Institute of Genetics, Japan). The obtained PCR products and the knock-in cassette were cloned into pBluescriptII SK+ using the In-Fusion HD cloning kit (Takara Bio). The obtained knock-in construct was co-injected with the gRNA into the embryos of Cas9-expressing flies (NIG-FLY Stock Center CAS-0001) following a standard protocol for generating transgenic flies. Integration into the *sqh* locus was confirmed by sequencing.

### Live imaging

Staged pupae were washed in distilled water, and the pupal case covering about two-thirds of abdominal segments was removed. Pupae were mounted on coverslips with adhesive tape. Live imaging was carried out on a TCS SP5 confocal microscope (Leica), TCS SP5 inverted confocal microscope (Leica) or TCS SP8 inverted confocal microscope (Leica). Live imaging at the restrictive temperature was performed as follows. Pupae were raised at 18°C until 24 h APF, and then transferred to 29°C after removing pupal cases. Live imaging was performed at 29°C on a thermo plate (Tokai Hit Co., Shizuoka, Japan) from 30 h APF. Otherwise, pupae were raised at 25°C, and live imaging was performed at room temperature from 20 h APF.

### Image analysis

Images were processed with ImageJ software (NIH). z-projected images were used for analysis unless otherwise mentioned. Cell tracking was performed using the 'TrackMate' plugin in ImageJ (Tinevez et al., 2017). Cells in the second and third segments of the abdomen were tracked (Fig. 1B). Fluorescence intensity in *pnr*-expressing regions was normalized to mean intensity of non-*pnr*-expressing regions. Intensities were acquired from cells in the second segment of *pnr*-expressing regions and cells in the second segment of non-*pnr*-expressing regions. Pseudocolor images were acquired with MetaMorph software (Molecular Devices). For the quantification of vesicles of Clc::GFP, a planar section that contains the most abundant puncta was analyzed for each cell. Signals for the puncta were thresholded to distinguish them from weak signals. Particles larger than 100 nm<sup>2</sup> were counted using the 'Analyze Particles' function for each cell. For FRET analysis, ECFP and Venus channel backgrounds were removed with MetaMorph software, and the FRET ratio (Venus/ECFP) was measured with ImageJ. Caspase activation was detected as follows: the FRET ratio of living cells in the second segment of non-*pnr*-expressing region was measured; then the FRET ratio of fragmented cells derived from the second segment of non-*pnr*-expressing region was measured, and the numeric value between FRET ratios of living cells and of fragmented cells was set as the threshold of caspase activation. The FRET ratio of cells in the second and third segments of *pnr*-expressing region was measured, and once the numeric value exceeded the threshold, it was recorded as caspase activation.

### Area quantification

Live imaging data in which cells were labeled with Nrg-GFP were used for automated segmentation, cell tracking, and output of cellular parameters using the Tissue Analyzer plugin in Fiji software (<https://fiji.sc/>) (Aigouy et al., 2016). The segmentation images were hand-corrected for better representation of cell outlines. For the graphs comparing the area reduction of extruding cells, the area of quantified cells at each time point was normalized by their initial area. All the data were aligned at the time point when the area reached 75% of the initial area.

### Dextran uptake assay

To monitor fluid phase incorporation activity for LECs, properly staged pupal epidermal tissues were dissected and cultured in Schneider S2 cell

medium (Gibco) in the presence of 0.5 mg/ml dextran (10,000 MW) conjugated with Alexa555 (Thermo Fisher Scientific) for 10 min, followed by 30 min of incubation at 29°C without dextran in order to unambiguously distinguish signals from non-specific cuticular staining on the tissue surface and internalized vesicles. Samples were fixed with 4% paraformaldehyde and mounted in 50% glycerol.

### Image analysis for dextran uptake assay

For the quantification of vesicles having incorporated dextran-Alexa555, a planar section containing the most abundant puncta was analyzed for each cell. Image processing was performed in Fiji. Signals for the puncta were thresholded to distinguish them from weak signals, which most likely accumulated in lysosomes and background staining outside of the cells. Background signal was further removed using the ‘Open’ function in the binary operation. Particles larger than 100 nm<sup>2</sup> were counted using the ‘Analyze Particles’ function for each cell.

### Statistics

All statistics and graphs were performed in R version 3.5.1 (The R Foundation for Statistical Computing). The analyses for duration of area reduction for extruding LECs were compared with a Mann–Whitney U test. The quantification of Clc::GFP puncta was compared using a Mann–Whitney U test. The time course analyses of the fraction of remaining LECs were compared with a Kolmogorov–Smirnov test. The intensity of E-cadherin signal was compared with a Tukey test. The intensity of Myosin II signal was compared with a Games–Howell test.

### Acknowledgements

We thank Yang Hong, Marko Brankatschk, Enrique Martín-Blanco, the NIG-FLY Stock Center and the Bloomington *Drosophila* Stock Center; Shu Kondo for providing a vector for CRISPR/Cas9 mediated knock-in DNA construction; and Yuichiro Nakajima and Hiroyuki Uechi, Hironobu Fijita and Tomohiko Taguchi for useful discussions.

### Author contributions

Conceptualization: S.H., D.U.; Validation: D.U.; Formal analysis: S.H., X.S., D.U.; Investigation: S.H., X.S., D.U.; Resources: E.K.; Writing - original draft: D.U.; Writing - review & editing: D.U.; Visualization: S.H., X.S., D.U.; Supervision: D.U.; Project administration: D.U.; Funding acquisition: E.K., D.U.

### Competing interests

The authors declare no competing or financial interests.

### Funding

This work was supported by the Japan Science and Technology Agency CREST program (JPMJCR1852 to E.K.), a research grant from Astellas Foundation for Research on Metabolic Disorders (J170002241 to E.K.), Japan Society for the Promotion of Science (JP24687027, JP16H04800 to E.K.; JP15K18536, JP17K07402, JP17H02939 to D.U.) and Grants-in-Aid for Scientific Research from the Ministry of Education, Culture, Sports, Science and Technology (JP26114003 to E.K.).

### Supplementary information

Supplementary information available online at <http://dev.biologists.org/lookup/doi/10.1242/dev.179648.supplemental>

### References

- Aigouy, B., Umetsu, D. and Eaton, S. (2016). Segmentation and quantitative analysis of epithelial tissues. *Methods Mol. Biol.* **1478**, 227–239. doi:10.1007/978-1-4939-6371-3\_13
- Amcheslavsky, A., Wang, S., Fogarty, C. E., Lindblad, J. L., Fan, Y. and Bergmann, A. (2018). Plasma membrane localization of apoptotic caspases for non-apoptotic functions. *Dev. Cell* **45**, 450–464.e3. doi:10.1016/j.devcel.2018.04.020
- Arata, M., Sugimura, K. and Uemura, T. (2017). Difference in dachsous levels between migrating cells coordinates the direction of collective cell migration. *Dev. Cell* **42**, 479–497.e10. doi:10.1016/j.devcel.2017.08.001
- Austin, C. D., Lawrence, D. A., Peden, A. A., Varfolomeev, E. E., Totpal, K., De Maziere, A. M., Klumperman, J., Arnott, D., Pham, V., Scheller, R. H. et al. (2006). Death-receptor activation halts clathrin-dependent endocytosis. *Proc. Natl Acad. Sci. USA* **103**, 10283–10288. doi:10.1073/pnas.0604044103
- Bannerman, D. D., Sathyamoorthy, M. and Goldblum, S. E. (1998). Bacterial lipopolysaccharide disrupts endothelial monolayer integrity and survival signaling events through caspase cleavage of adherens junction proteins. *J. Biol. Chem.* **273**, 35371–35380. doi:10.1074/jbc.273.52.35371
- Bardet, P.-L., Kolahgar, G., Mynett, A., Miguel-Aliaga, I., Briscoe, J., Meier, P. and Vincent, J.-P. (2008). A fluorescent reporter of caspase activity for live imaging. *Proc. Natl. Acad. Sci. USA* **105**, 13901–13905. doi:10.1073/pnas.0806983105
- Bischoff, M. (2012). Lamellipodia-based migrations of larval epithelial cells are required for normal closure of the adult epidermis of *Drosophila*. *Dev. Biol.* **363**, 179–190. doi:10.1016/j.ydbio.2011.12.033
- Brancolini, C., Lazarevic, D., Rodriguez, J. and Schneider, C. (1997). Dismantling cell-cell contacts during apoptosis is coupled to a caspase-dependent proteolytic cleavage of  $\beta$ -catenin. *J. Cell Biol.* **139**, 759–771. doi:10.1083/jcb.139.3.759
- Brás-Pereira, C. and Moreno, E. (2018). Mechanical cell competition. *Curr. Opin. Cell Biol.* **51**, 15–21. doi:10.1016/j.ceb.2017.10.003
- Bucci, C., Parton, R. G., Mather, I. H., Stunnenberg, H., Simons, K., Hoflack, B. and Zerial, M. (1992). The small GTPase rab5 functions as a regulatory factor in the early endocytic pathway. *Cell* **70**, 715–728. doi:10.1016/0092-8674(92)90306-W
- Calleja, M., Moreno, E., Pelaz, S. and Morata, G. (1996). Visualization of gene expression in living adult *Drosophila*. *Science* **274**, 252–255. doi:10.1126/science.274.5285.252
- Chandraratna, D., Lawrence, N., Welchman, D. P. and Sanson, B. (2007). An in vivo model of apoptosis: Linking cell behaviours and caspase substrates in embryos lacking DIAP1. *J. Cell Sci.* **120**, 2594–2608. doi:10.1242/jcs.03472
- Classen, A. K., Anderson, K. I., Marois, E. and Eaton, S. (2005). Hexagonal packing of *Drosophila* wing epithelial cells by the planar cell polarity pathway. *Dev. Cell* **9**, 805–817. doi:10.1016/j.devcel.2005.10.016
- Clevers, H., Loh, K. M. and Nusse, R. (2014). An integral program for tissue renewal and regeneration: Wnt signaling and stem cell control. *Science* **346**, 1248012. doi:10.1126/science.1248012
- De La Cova, C., Abril, M., Bellosta, P., Gallant, P. and Johnston, L. A. (2004). *Drosophila* myc regulates organ size by inducing cell competition. *Cell* **117**, 107–116. doi:10.1016/S0092-8674(04)00214-4
- Desai, R., Sarpal, R., Ishiyama, N., Pellicka, M., Ikura, M. and Tepass, U. (2013). Monomeric  $\alpha$ -catenin links cadherin to the actin cytoskeleton. *Nat. Cell Biol.* **15**, 261–273. doi:10.1038/ncb2685
- Dunst, S., Kazimiers, T., von Zadow, F., Jambor, H., Sagner, A., Brankatschk, B., Mahmoud, A., Spann, S., Tomancak, P., Eaton, S. et al. (2015). Endogenously tagged rab proteins: a resource to study membrane trafficking in *Drosophila*. *Dev. Cell* **33**, 351–365. doi:10.1016/j.devcel.2015.03.022
- Fischer, J. A., Eun, S. H. and Doolan, B. T. (2006). Endocytosis, endosome trafficking, and the regulation of *Drosophila* development. *Annu. Rev. Cell Dev. Biol.* **22**, 181–206. doi:10.1146/annurev.cellbio.22.010605.093205
- Fukata, Y., Kimura, K., Oshiro, N., Saya, H., Matsuura, Y. and Kaibuchi, K. (1998). Association of the myosin-binding subunit of myosin phosphatase and moesin: dual regulation of moesin phosphorylation by Rho-associated kinase and myosin phosphatase. *J. Cell Biol.* **141**, 409–418. doi:10.1083/jcb.141.2.409
- Georgiou, M., Marinari, E., Burden, J. and Baum, B. (2008). Cdc42, Par6, and aPKC regulate Arp2/3-mediated endocytosis to control local adherens junction stability. *Curr. Biol.* **18**, 1631–1638. doi:10.1016/j.cub.2008.09.029
- Goetzl, E. J. and An, S. (1998). Diversity of cellular receptors and functions for the lysophospholipid growth factors lysophosphatidic acid and sphingosine 1-phosphate. *FASEB J.* **12**, 1589–1598. doi:10.1096/fasebj.12.15.1589
- Grigliatti, T. A., Hall, L., Rosenbluth, R. and Suzuki, D. T. (1973). Temperature-sensitive mutations in *Drosophila melanogaster*: XIV. A selection of immobile adults. *Mol. Gen. Genet.* **120**, 107–114. doi:10.1007/BF00267238
- Gudipaty, S. A. and Rosenblatt, J. (2017). Epithelial cell extrusion: pathways and pathologies. *Semin. Cell Dev. Biol.* **67**, 132–140. doi:10.1016/j.semcb.2016.05.010
- Hay, B. A., Wassarman, D. A. and Rubin, G. M. (1995). *Drosophila* homologs of baculovirus inhibitor of apoptosis proteins function to block cell death. *Cell* **83**, 1253–1262. doi:10.1016/0092-8674(95)90150-7
- Herskovits, J. S., Burgess, C. C., Obar, R. A. and Vallee, R. B. (1993). Effects of mutant rat dynamin on endocytosis. *J. Cell Biol.* **122**, 565–578. doi:10.1083/jcb.122.3.565
- Huang, J., Zhou, W., Dong, W., Watson, A. M. and Hong, Y. (2009). Directed, efficient, and versatile modifications of the *Drosophila* genome by genomic engineering. *Proc. Natl Acad. Sci. USA* **106**, 8284–8289. doi:10.1073/pnas.0900641106
- Igaki, T., Pastor-Pareja, J. C., Aonuma, H., Miura, M. and Xu, T. (2009). Intrinsic tumor suppression and epithelial maintenance by endocytic activation of eiger/ TNF signaling in *Drosophila*. *Dev. Cell* **16**, 458–465. doi:10.1016/j.devcel.2009.01.002
- Iyer, K. V., Piscitello-Gómez, R., Pajmans, J., Jülicher, F. and Eaton, S. (2019). Epithelial viscoelasticity is regulated by mechanosensitive e-cadherin turnover. *Curr. Biol.* **29**, 578–591.e5. doi:10.1016/j.cub.2019.01.021
- Jewett, C. E., Vanderleest, T. E., Miao, H., Xie, Y., Madhu, R., Loerke, D. and Blankenship, J. T. (2017). Planar polarized Rab35 functions as an oscillatory



- ratchet during cell intercalation in the *Drosophila* epithelium. *Nat. Commun.* **8**, 897. doi:10.1038/s41467-017-00553-0
- Kamiguchi, H. and Lemmon, V.** (2000). Recycling of the cell adhesion molecule L1 in axonal growth cones. *J. Neurosci.* **20**, 3676-3686. doi:10.1523/JNEUROSCI.20-10-03676.2000
- Kanuka, H., Kuranaga, E., Takemoto, K., Hiratou, T., Okano, H. and Miura, M.** (2005). *Drosophila* caspase transduces Shaggy/GSK-3 $\beta$  kinase activity in neural precursor development. *EMBO J.* **24**, 3793-3806. doi:10.1038/sj.emboj.7600822
- Kessler, T. and Müller, H. A. J.** (2009). Cleavage of armadillo/beta-catenin by the caspase DrlCE in *drosophila* apoptotic epithelial cells. *BMC Dev. Biol.* **9**, 251. doi:10.1186/1471-213X-9-15
- Kitamoto, T.** (2001). Conditional modification of behavior in *drosophila* by targeted expression of a temperature-sensitive shibire allele in defined neurons. *J. Neurobiol.* **47**, 81-92. doi:10.1002/neu.1018
- Kjøller, L. and Hall, A.** (1999). Signaling to Rho GTPases. *Exp. Cell Res.* **253**, 166-179. doi:10.1006/excr.1999.4674
- Kondo, S. and Ueda, R.** (2013). Highly Improved gene targeting by germline-specific Cas9 expression in *Drosophila*. *Genetics* **195**, 715-721. doi:10.1534/genetics.113.156737
- Koto, A., Kuranaga, E. and Miura, M.** (2009). Temporal regulation of *Drosophila* IAP1 determines caspase functions in sensory organ development. *J. Cell Biol.* **187**, 219-231. doi:10.1083/jcb.200905110
- Lai, S.-L. and Lee, T.** (2006). Genetic mosaic with dual binary transcriptional systems in *Drosophila*. *Nat. Neurosci.* **9**, 703-709. doi:10.1038/nn1681
- Langemeyer, L., Fröhlich, F. and Ungermann, C.** (2018). Rab GTPase function in endosome and lysosome biogenesis. *Trends Cell Biol.* **28**, 957-970. doi:10.1016/j.tcb.2018.06.007
- Lee, A. and Treisman, J. E.** (2004). Excessive Myosin activity in mbs mutants causes photoreceptor movement out of the *Drosophila* eye disc epithelium. *Mol. Biol. Cell* **15**, 3285-3295. doi:10.1091/mbc.E04
- Lee, J.-Y. and Harland, R. M.** (2010). Endocytosis is required for efficient apical constriction during *Xenopus* gastrulation. *Curr. Biol.* **20**, 253-258. doi:10.1016/j.cub.2009.12.021
- Levayer, R., Pelissier-Monier, A. and Lecuit, T.** (2011). Spatial regulation of Dia and Myosin-II by RhoGEF2 controls initiation of E-cadherin endocytosis during epithelial morphogenesis. *Nat. Cell Biol.* **13**, 529-540. doi:10.1038/ncb2224
- Levayer, R., Dupont, C. and Moreno, E.** (2016). Tissue crowding induces caspase-dependent competition for space. *Curr. Biol.* **26**, 670-677. doi:10.1016/j.cub.2015.12.072
- Lubkov, V. and Bar-Sagi, D.** (2014). E-cadherin-mediated cell coupling is required for apoptotic cell extrusion. *Curr. Biol.* **24**, 868-874. doi:10.1016/j.cub.2014.02.057
- Madhavan, M. M. and Madhavan, K.** (1980). Morphogenesis of the epidermis of adult abdomen of *Drosophila*. *J. Embryol. Exp. Morphol.* **60**, 1-31.
- Malliri, A., Symons, M., Hennigan, R. F., Hurlstone, A. F. L., Lamb, R. F., Wheeler, T. and Ozanne, B. W.** (1998). The transcription factor AP-1 is required for EGF-induced activation of Rho-like GTPases, cytoskeletal rearrangements, motility, and in vitro invasion of A431 cells. *J. Cell Biol.* **143**, 1087-1099. doi:10.1083/jcb.143.4.1087
- Maruyama, T. and Fujita, Y.** (2017). Cell competition in mammals — novel homeostatic machinery for embryonic development and cancer prevention. *Curr. Opin. Cell Biol.* **48**, 106-112. doi:10.1016/j.cob.2017.06.007
- Mcsharry, S. S. and Beitel, G. J.** (2019). The Caspase-3 homolog DrlCE regulates endocytic trafficking during *Drosophila* tracheal morphogenesis. *Nat. Commun.* **10**, 382. doi:10.1038/s41467-019-09009-z
- Merino, M. M., Levayer, R. and Moreno, E.** (2016). Survival of the fittest: essential roles of cell competition in development, aging, and cancer. *Trends Cell Biol.* **26**, 776-788. doi:10.1016/j.tcb.2016.05.009
- Minambres, R.** (2006). The RhoA/ROCK-1/MLC pathway is involved in the ethanol-induced apoptosis by anoikis in astrocytes. *J. Cell Sci.* **119**, 271-282. doi:10.1242/jcs.02723
- Moreno, E., Valon, L., Levillayer, F. and Levayer, R.** (2019). Competition for space induces cell elimination through compaction-driven ERK downregulation. *Curr. Biol.* **29**, 23-34.e8. doi:10.1016/j.cub.2018.11.007
- Moreno, E. and Basler, K.** (2004). dMyc transforms cells into super-competitors. *Cell* **117**, 117-129. doi:10.1016/S0092-8674(04)00262-4
- Nakajima, Y.-I., Kuranaga, E., Sugimura, K., Miyawaki, A. and Miura, M.** (2011). Nonautonomous apoptosis is triggered by local cell cycle progression during epithelial replacement in *Drosophila*. *Mol. Cell Biol.* **31**, 2499-2512. doi:10.1128/mcb.01046-10
- Ninon, N., Chiarelli, D. A. and Martin-Blanco, E.** (2007). Extrinsic and intrinsic mechanisms directing epithelial cell sheet replacement during *Drosophila* metamorphosis. *Development* **134**, 367-379. doi:10.1242/dev.02728
- Ohswa, S., Vaughan, J. and Igaki, T.** (2018). Cell extrusion: a stress-responsive force for good or evil in epithelial homeostasis. *Dev. Cell* **44**, 284-296. doi:10.1016/j.devcel.2018.01.009
- Okumura, N., Fujii, K., Kagami, T., Makiko, N., Kitahara, M., Kinoshita, S. and Koizumi, N.** (2016). Activation of the rho/rho kinase signaling pathway is involved in cell death of corneal endothelium. *Invest. Ophthalmol. Vis. Sci.* **57**, 6843. doi:10.1167/iovs.16-20123
- Palecek, S. P., Schmidt, C. E., Lauffenburger, D. A. and Horwitz, A. F.** (1996). Integrin dynamics on the tail region of migrating fibroblasts. *J. Cell Sci.* **109**, 941-952.
- Petrache, I., Verin, A. D., Crow, M. T., Birukova, A., Liu, F. and Garcia, J. G. N.** (2001). Differential effect of MLC kinase in TNF- $\alpha$ -induced endothelial cell apoptosis and barrier dysfunction. *Am. J. Physiol. Lung Cell. Mol. Physiol.* **280**, L1168-L1178. doi:10.1152/ajplung.2001.280.6.L1168
- Petrache, I., Crow, M. T., Neuss, M. and Garcia, J. G. N.** (2003). Central involvement of Rho family GTPases in TNF- $\alpha$ -mediated bovine pulmonary endothelial cell apoptosis. *Biochem. Biophys. Res. Commun.* **306**, 244-249. doi:10.1016/S0006-291X(03)00945-8
- Puls, A., Eliopoulos, A. G., Nobes, C. D., Bridges, T., Young, L. S. and Hall, A.** (1999). Activation of the small GTPase Cdc42 by the inflammatory cytokines TNF(alpha) and IL-1, and by the Epstein-Barr virus transforming protein LMP1. *J. Cell Sci.* **112**, 2983-2992.
- Röper, K.** (2015). Integration of cell-cell adhesion and contractile actomyosin activity during morphogenesis. *Curr. Top. Dev. Biol.* **112**, 103-127. doi:10.1016/bs.ctdb.2014.11.017
- Roseland, C. R. and Schneiderman, H. A.** (1979). Regulation and metamorphosis of the abdominal histoblasts of *Drosophila melanogaster*. *Wilhelm Roux's Arch. Dev. Biol.* **186**, 235-265. doi:10.1007/BF00848591
- Rossman, K. L., Der, C. J. and Sondek, J.** (2005). GEF means go: turning on Rho GTPases with guanine nucleotide-exchange factors. *Nat. Rev. Mol. Cell Biol.* **6**, 167-180. doi:10.1038/nrm1587
- Saitoh, S., Maruyama, T., Yako, Y., Kajita, M., Fujioka, Y., Ohba, Y., Kasai, N., Sugama, N., Kon, S., Ishikawa, S. et al.** (2017). Rab5-regulated endocytosis plays a crucial role in apical extrusion of transformed cells. *Proc. Natl Acad. Sci. USA* **114**, E2327-E2336. doi:10.1073/pnas.1602349114
- Saw, T. B., Doostmohammadi, A., Nier, V., Kocgozlu, L., Thampi, S., Toyama, Y., Marcq, P., Lim, C. T., Yeomans, J. M. and Ladoux, B.** (2017). Topological defects in epithelia govern cell death and extrusion. *Nature* **544**, 212-216. doi:10.1038/nature21718
- Sekyrova, P., Bohmann, D., Jindra, M. and Uhlírova, M.** (2010). Interaction between *Drosophila* ZIP proteins Atf3 and Jun prevents replacement of epithelial cells during metamorphosis. *Development* **137**, 141-150. doi:10.1242/dev.037861
- Seto, E. S., Bellen, H. J. and Lloyd, T. E.** (2002). When cell biology meets development: Endocytic regulation of signaling pathways. *Genes Dev.* **16**, 1314-1336. doi:10.1101/gad.989602
- Sigismund, S., Confalonieri, S., Ciliberto, A., Polo, S., Scita, G. and Di Fiore, P. P.** (2012). Endocytosis and signaling: cell logistics shape the eukaryotic cell plan. *Physiol. Rev.* **92**, 273-366. doi:10.1152/physrev.00005.2011
- Steinhilber, U., Weiske, J., Badock, V., Tauber, R., Bommert, K. and Huber, O.** (2001). Cleavage and shedding of E-cadherin after induction of apoptosis. *J. Biol. Chem.* **276**, 4972-4980. doi:10.1074/jbc.M006102200
- Takeichi, M.** (2014). Dynamic contacts: rearranging adherens junctions to drive epithelial remodeling. *Nat. Rev. Mol. Cell Biol.* **15**, 397-410. doi:10.1038/nrm3802
- Takemoto, K., Nagai, T., Miyawaki, A. and Miura, M.** (2003). Spatio-temporal activation of caspase revealed by indicator that is insensitive to environmental effects. *J. Cell Biol.* **160**, 235-243. doi:10.1083/jcb.200207111
- Teng, X., Qin, L., Le Borgne, R. and Toyama, Y.** (2017). Remodeling of adhesion and modulation of mechanical tensile forces during apoptosis in *Drosophila* epithelium. *J. Cell Sci.* **130**, e1.2. doi:10.1242/jcs.201343
- Tinevez, J. Y., Perry, N., Schindelin, J., Hoopes, G. M., Reynolds, G. D., Laplantine, E., Bednarek, S. Y., Shorte, S. L. and Eliceiri, K. W.** (2017). TrackMate: an open and extensible platform for single-particle tracking. *Methods* **115**, 80-90. doi:10.1016/j.ymeth.2016.09.016
- Twomey, J. D., Kim, S.-R., Zhao, L., Bozza, W. P. and Zhang, B.** (2015). Spatial dynamics of TRAIL death receptors in cancer cells. *Drug Resist. Updates* **19**, 13-21. doi:10.1016/j.drug.2015.02.001
- Vaccari, T. and Bilder, D.** (2009). At the crossroads of polarity, proliferation and apoptosis: the use of *Drosophila* to unravel the multifaceted role of endocytosis in tumor suppression. *Mol. Oncol.* **3**, 354-365. doi:10.1016/j.molonc.2009.05.005
- Van Der Bliek, A. M., Redelmeier, T. E., Damke, H., Tisdale, E. J., Meyerowitz, E. M. and Schmid, S. L.** (1993). Mutations in human dynamin block an intermediate stage in coated vesicle formation. *J. Cell Biol.* **122**, 553-563. doi:10.1083/jcb.122.3.553
- Vanlandingham, P. A. and Ceresa, B. P.** (2009). Rab7 regulates late endocytic trafficking downstream of multivesicular body biogenesis and cargo sequestration. *J. Biol. Chem.* **284**, 12110-12124. doi:10.1074/jbc.M809277200
- Vasquez, C. G. and Martin, A. C.** (2016). Force transmission in epithelial tissues. *Dev. Dyn.* **245**, 361-371. doi:10.1002/dvdy.24384
- Wells, J. M. and Watt, F. M.** (2018). Diverse mechanisms for endogenous regeneration and repair in mammalian organs. *Nature* **557**, 322-328. doi:10.1038/s41586-018-0073-7
- Yamada, S., Pokutta, S., Drees, F., Weis, W. I. and Nelson, W. J.** (2005). Deconstructing the cadherin-catenin-actin complex. *Cell* **123**, 889-901. doi:10.1016/j.cell.2005.09.020
- Zhang, Y. and Zhang, B.** (2008). TRAIL resistance of breast cancer cells is associated with constitutive endocytosis of death receptors 4 and 5. *Mol. Cancer Res.* **6**, 1861-1871. doi:10.1158/1541-7786.mcr-08-0313

## Supplementary Information

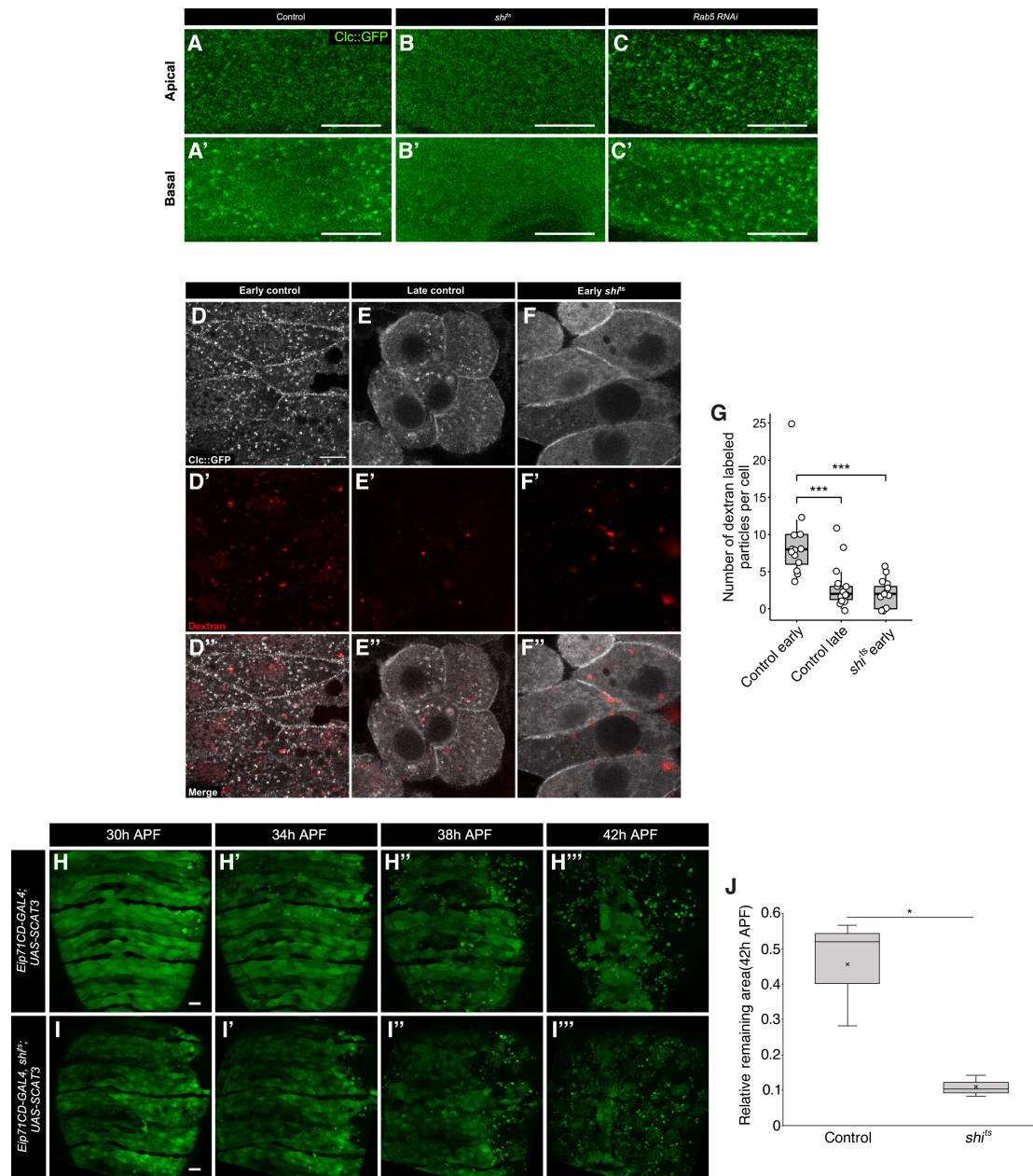


**Figure S1. Endocytic activity reduces as tissue remodeling progresses during metamorphosis**

(A-C) Clc::GFP puncta as a marker for endocytic activity in RT control (A), *shi<sup>ts</sup>* expressing (B), and *Rab5* RNAi (C) LECs. Anterior is up. Scale bar: 10  $\mu$ m. Note that the number of puncta was dramatically reduced for *shi<sup>ts</sup>* expressing cells, and numerous smaller puncta accumulated for *Rab5* RNAi, which is consistent with the reported phenotype for *Rab5* inhibition (Bucci *et al.*, 1992).

(D-F) Dextran uptake for RT control at the early stage (D), the late stage (E), and *shits* at the early stage (F). Clc::GFP (white) and dextran (red) are shown.

(G) Quantification of the number of dextran labeled vesicles per cell (control early: N = 13 cells, control late: N = 14, *shits*: N = 13 Mann-Whitney *U* test, \*\*\* $p < 0.001$ ).

(H-I) Time course of the LEC elimination for RT control (H) and *shits* expressing (I) LECs under the control of an Eip71CD-GAL4 driver under the restrictive temperature at different time points indicated above. Anterior is up. Scale bar: 50  $\mu\text{m}$ .

(J) Quantification of the area of GFP expression domain at the time point 42 hours APF relative to 30 hours APF. Student's *t* test. \* $p < 0.05$ . N = 4 pupae for each experiment.



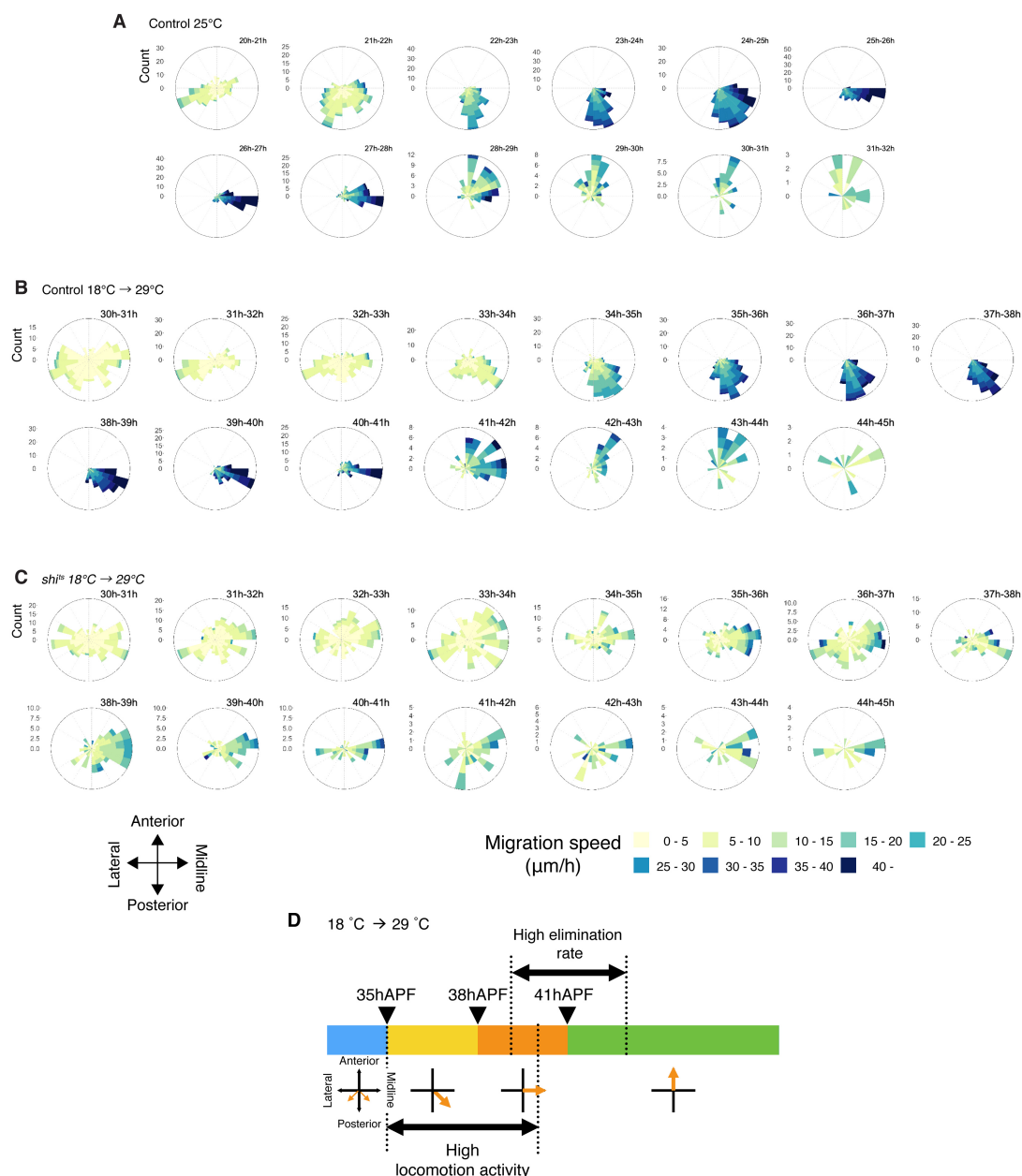


**Figure S2. Reduction of endocytic activity affects migration of LECs**

(A) Time course analysis of LEC migration orientation for control at 25°C .

(B-C) Time course analysis of LEC migration orientation for RT control (B) and *shi<sup>ts</sup>* expressing (C) LECs under the restriction temperature regime.

(D) Timeline of the high elimination phase with respect to the migration pattern of the LECs under the restriction temperature regime. Color code (blue, yellow, orange and green) represents different developmental time windows from early to late stages based on the locomotion activity and orientation of migration. Times (after puparium

formation) of transition are indicated on top. Note that the developmental time windows in the restriction temperature regime roughly correspond to that of a standard condition (25°C, Figure 1G). Orange arrows indicate orientation of the LEC migration at each time window. The time periods of high locomotion activity and high elimination rate are indicated below and above, respectively.



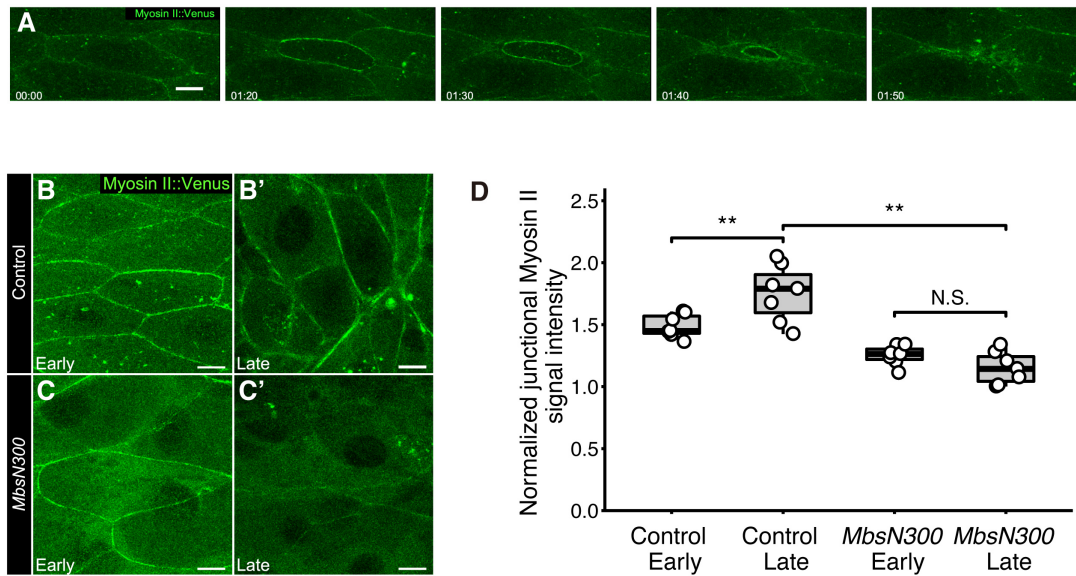


**Figure S3. Reduction of cortical Myosin II in the late stage caused by the over-expression of *MbsN300***

(A) Still images for subcellular localization of myosin II tagged with Venus (MyoII::Venus) during apical constriction-driven cell elimination in RT control. Anterior is up. Scale bar: 10  $\mu$ m.

(B-C) Subcellular localization of MyoII::Venus for control (B) and *MbsN300* expressing (C) LECs at the early (B, C) and late (B', C') stage. Note that the cortical localization of Myosin II is still visible at the early stage (C) but severely reduced at the late stage (C') upon over-expression of *MbsN300*.

(D) Signal intensity for MyoII::Venus at cell junctions normalized to that of cytoplasmic region for individual cells. Student's t-test,  $**p < 0.01$ .

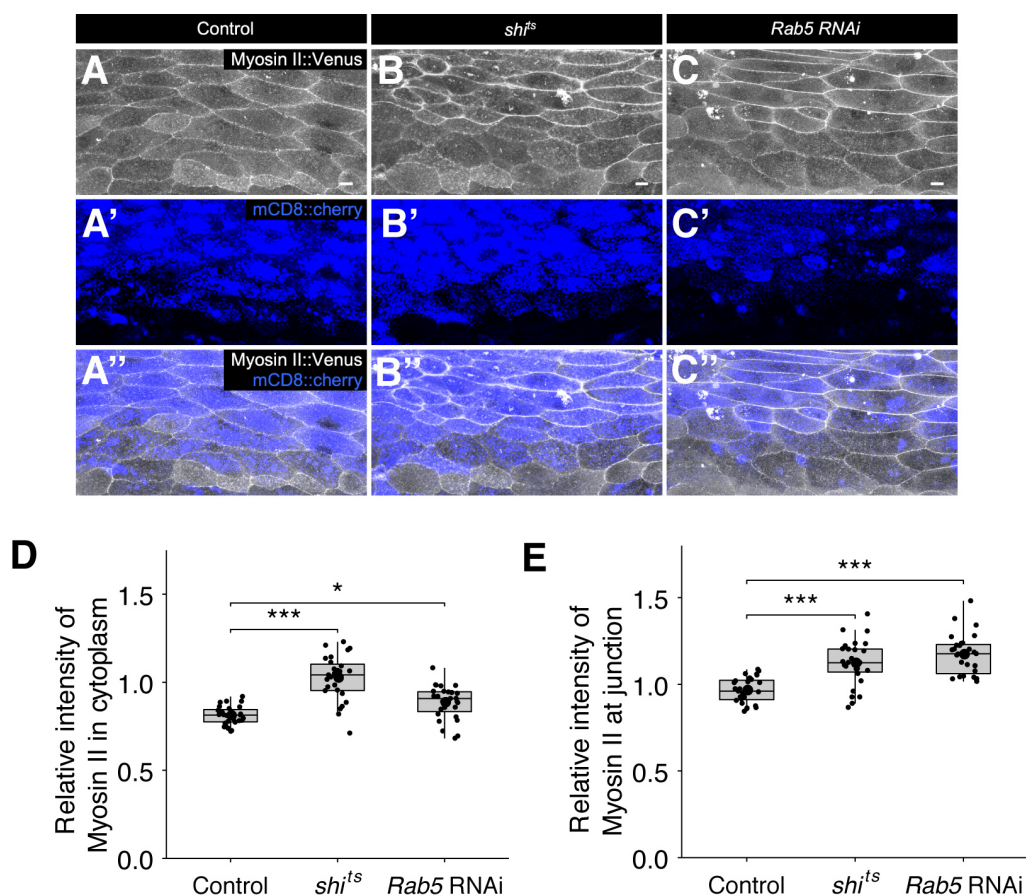


### Figure S4. Myosin II levels are elevated in LECs with reduced endocytic activity

(A-C) Subcellular localization of MyoII::Venus in RT control (A), *shi<sup>ts</sup>* expressing (B) and *Rab5* RNAi (C) LECs. Marker expression (mCD8::cherry) indicates the region of GAL4 expression (A', A'' B', B'' C', C''). Anterior is up. Scale bar: 10  $\mu$ m.

(D-E) Quantification of signal intensity of MyoII::Venus in the RT control, *shi<sup>ts</sup>* expressing and *Rab5* RNAi LECs relative to control region (*i.e.* non-GAL4 expression region) in each pupa for medial (D) and junctional (E) localization. One-way ANOVA followed by *post hoc* Games-Howell test. \* $p < 0.05$ , \*\*\* $p < 0.001$ . N = 3 pupae, 27 cells each.

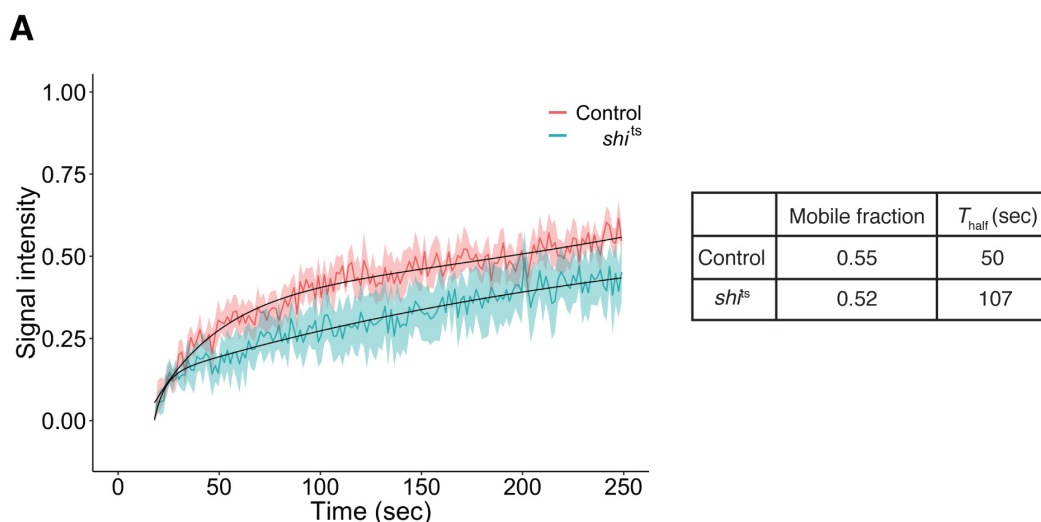


**Figure S5. Turn-over of E-cadherin in control and  $shi^{ts}$  LECs**

(A) Mobility of E-cadherin was analyzed by fluorescent recovery after photobleaching (FRAP) for RT control (red) and  $shi^{ts}$  expressing LECs (blue). A double exponential formula was used to fit the model to experimental results (black lines) to estimate the mobile fraction and the halftime of recovery  $T_{\text{half}}$ . E-cadherin::GFP was used for FRAP experiments. Staged control and  $shi^{ts}$  pupae were imaged by TCS SP8 confocal microscope (Leica) with 63 $\times$  oil objective lens with 2.0x zoom, under 10-20% 488nm laser. 30-32h APF pupae were used for the early stage, and late stage pupae were 40-42h APF. An about  $5 \times 2 \mu\text{m}$  region was selected for photobleaching with 100% intensity 488 nm laser for 0.653 seconds. Manually selected non-fluorescence area and total fluorescence area were used for normalization for each cell. Images were acquired with 0.5 seconds time intervals. Obtained dataset were averaged and then analyzed by fitting a double exponential formula:

$$I(t) = I_0 - \alpha \cdot e^{-\beta \cdot t} - \gamma \cdot e^{-\delta \cdot t}$$

$$\text{Mobile fraction} = I_0, \quad T_{\text{half}} = \frac{\ln(2)}{\beta}$$

The mobile fraction and the  $T_{\text{half}}$  are indicated in the table. Control: N = 10,  $shi^{ts}$ : N = 9.



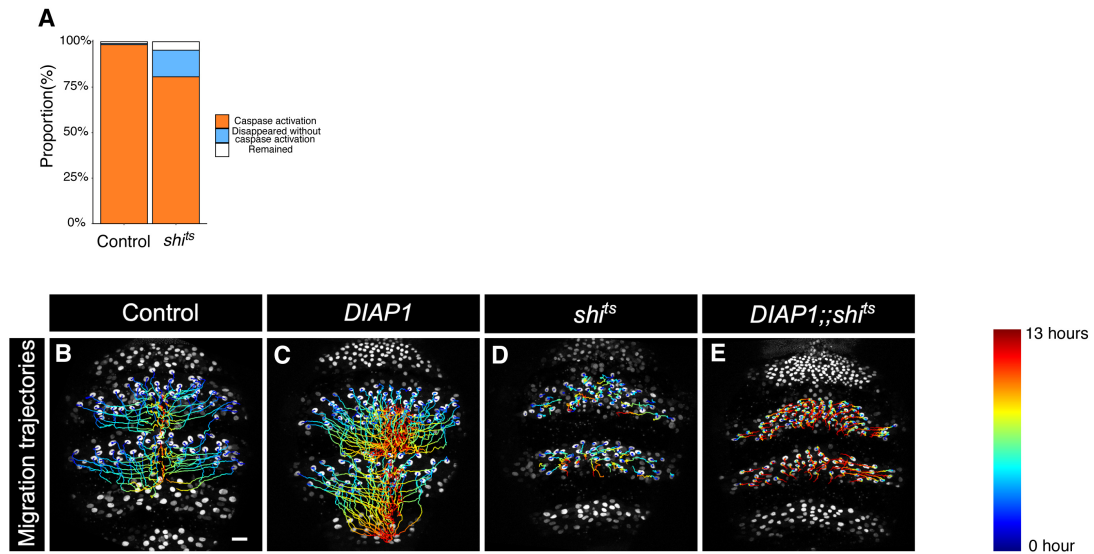


**Figure S6. Caspase activation-associated LEC elimination and cell elimination independent migration of endocytic defective LECs**

(A) Fraction of FRET signal positive cells among all dying cells for RT control and *shi<sup>ts</sup>* expressing LECs.

(B-E) Migration trajectories of LECs for RT control (B), DIAP over-expressing (C), *shi<sup>ts</sup>* expressing (D), and *shi<sup>ts</sup>* and DIAP over-expressing (E) pupae under the restrictive temperature.

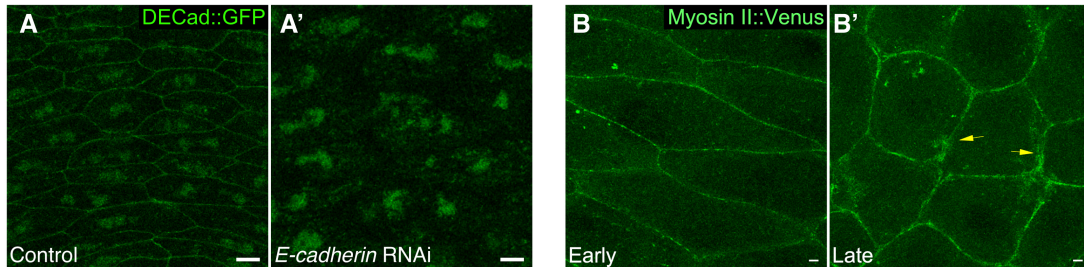


**Figure S7. E-cadherin RNAi effectively reduces E-cadherin levels and Myosin II is not regulated by caspase activation**

(A) E-cadherin::GFP in the LECs upon E-cadherin RNAi. Junctional E-cadherin signals are strongly reduced. Anterior is up. Scale bar: 10  $\mu$ m.

(B) MyoII::Venus reorganization at the late stage is unaffected by the over-expression of *DIAP1*. Yellow arrows indicate thick cortical accumulation of MyoII::Venus. Anterior is up. Scale bar: 10  $\mu$ m.

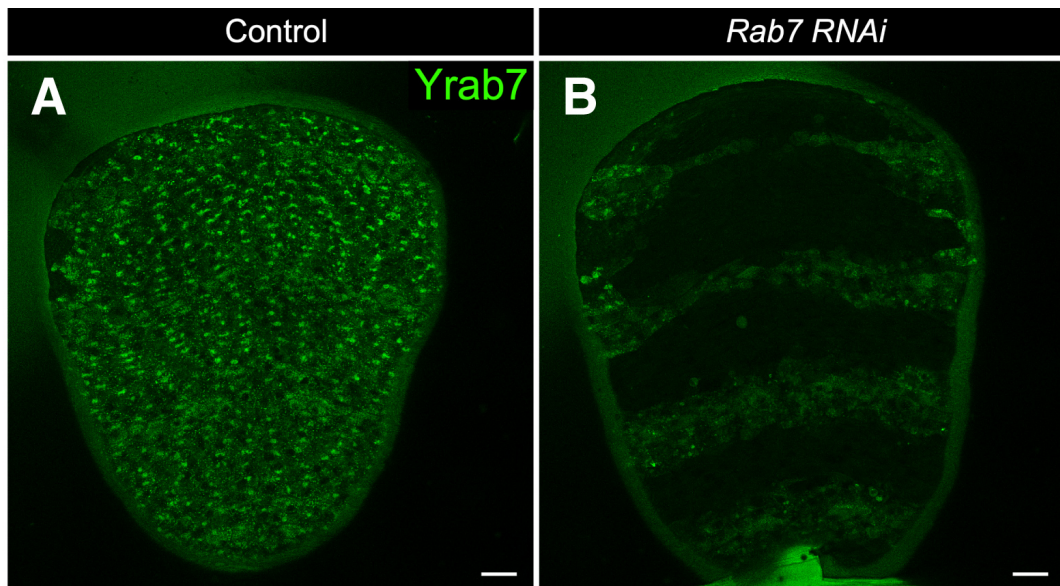


**Figure S8. Reduction of Rab7 protein by *Rab7* RNAi**

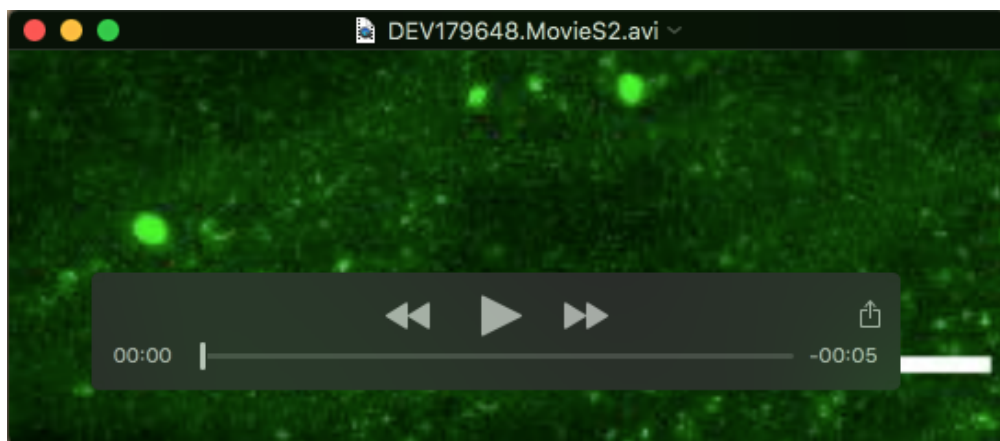
(A-B) Rab7::YFP knock-in (Dunst, Kazimiers, Eaton, *et al.*, 2015) for control (A) and *Rab7* RNAi (B) pupae. Anterior is up. Scale bar: 50  $\mu$ m.





**Movie 1. The elimination of LECs accelerates in the late stage of the tissue remodeling process**

Live imaging of the elimination of the LECs, labeled by the nuclear localized CFP::Venus under the control of *pnr*-GAL4 driver at 25°C. Dorsal view. Anterior is up. Scale bar: 50  $\mu$ m. Time interval: 10 min.



**Movie 2. The number of Clc::GFP puncta reduces as tissue remodeling progresses**

Live imaging of endocytic activity in the LECs using Clc::GFP as a marker. Although GFP signal is uniformly distributed in the cytoplasm, the number of GFP puncta gradually decreases over time. Note that eliminated cells also have much stronger accumulation of GFP puncta, which is the post-process of cell elimination and therefore irrelevant to the analysis of this study. Dorsal view. Anterior is up. Scale bar: 10  $\mu$ m. Time interval: 5 min.



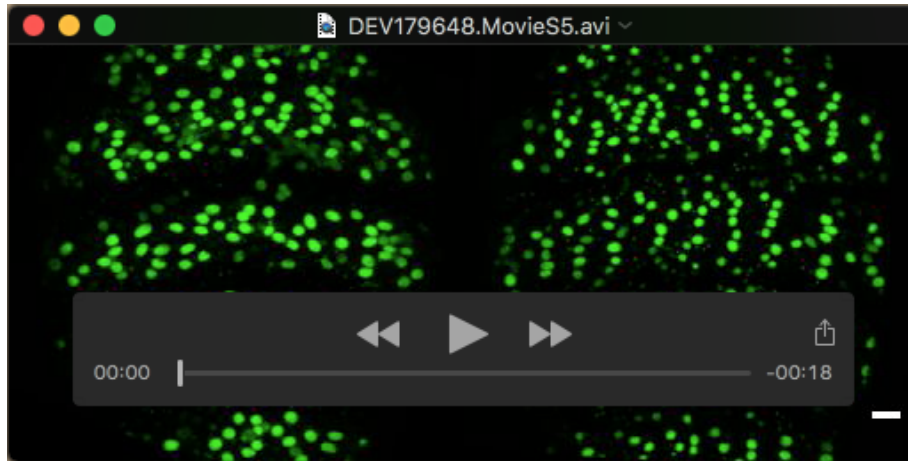
### Movie 3. Expression of *shits* in the LECs promotes cell elimination

Live imaging of the LEC elimination from pupae under the restrictive temperature (raised at 18°C, then shifted to 29°C at 6 hours before imaging) for RT control (left) and *shits* expressing (right) LECs. Dorsal view. Anterior is up. Scale bar: 50  $\mu$ m. Time interval: 10 min.



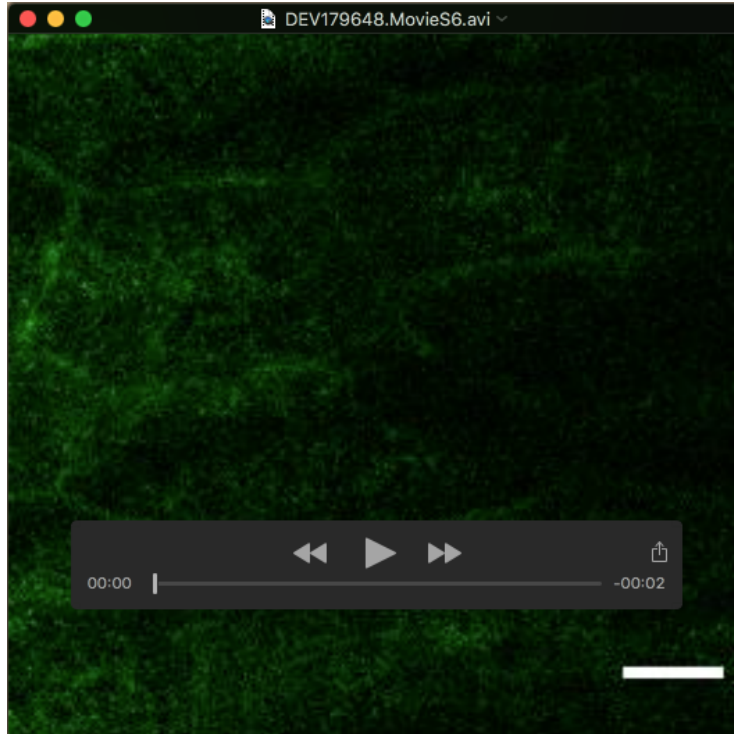
### Movie 4. Induction of *Rab5* RNAi in the LECs promotes cell elimination

Live imaging of the LEC elimination from pupae under the restrictive temperature (raised at 18°C, then shifted to 29°C at 6 hours before imaging) for RT control (left) and *Rab5* RNAi (right) LECs. Dorsal view. Anterior is up. Scale bar: 50  $\mu$ m. Time interval: 10 min.



**Movie 5. Over-expression of the Myosin II phosphatase *MbsN300* in the LECs diminishes the acceleration of cell elimination in the late stage**

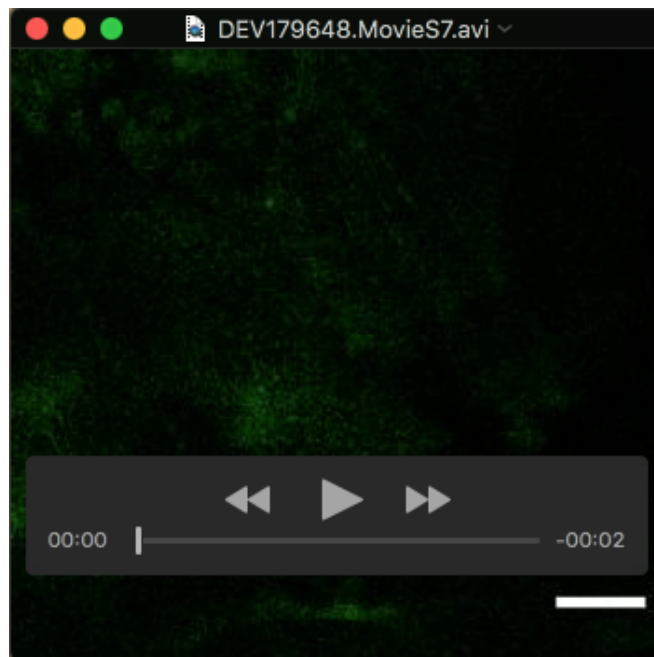
Live imaging of LEC elimination in pupa for control (left) and cells expressing Myosin phosphatase catalytic domain, *MbsN300* (right) at 25°C. Dorsal view. Anterior is up. Scale bar: 50  $\mu\text{m}$ . Time interval: 10 min.



**Movie 6. LECs in the early stage display Myosin II localization at the apical region**

Z-slice stack of MyoII::Venus in the LECs at the early stage for RT control (30h APF). Scale bar: 10  $\mu\text{m}$ . Z-slice interval: 0.75  $\mu\text{m}$ .

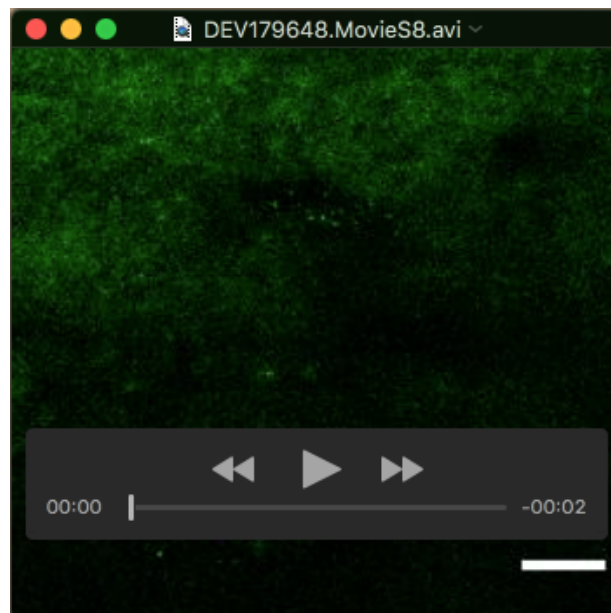




**Movie 7. LECs in the late stage display strong Myosin II localization**

Z-slice stack of MyoII::Venus in the LECs at the early stage for RT control (40h APF).

Scale bar: 10  $\mu$ m. Z-slice interval: 0.75  $\mu$ m.



**Movie 8. *shi*<sup>ts</sup> expressing LECs in the early stage display strong Myosin II localization**

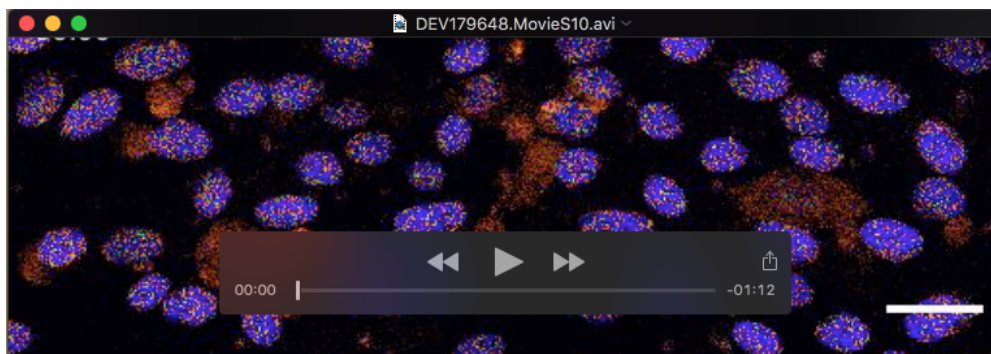
Z-slice stack of MyoII::Venus in the LECs at the early stage for *shi*<sup>ts</sup> (30h APF). Scale bar:

10  $\mu$ m. Z-slice interval: 0.75  $\mu$ m.



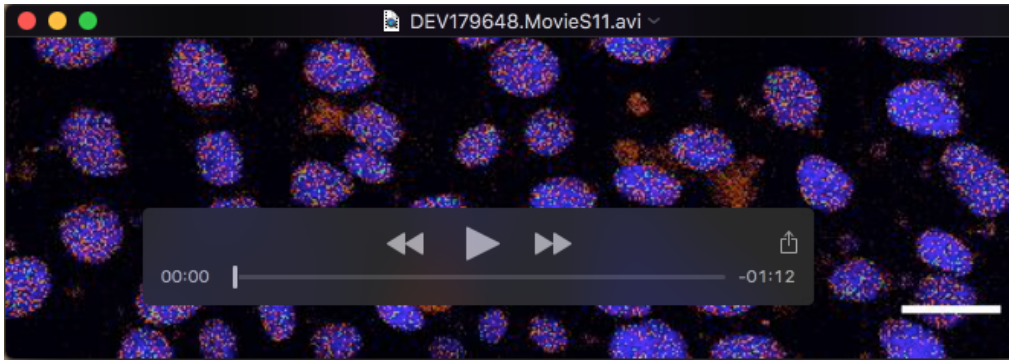
**Movie 9. *shi*<sup>ts</sup> expressing LECs in the late stage display strong Myosin II localization**

Z-slice stack of MyoII::Venus in the LECs at the early stage for *shi*<sup>ts</sup> (40h APF). Scale bar: 10  $\mu$ m. Z-slice interval: 0.75  $\mu$ m.



**Movie 10. Caspase activation is observed before fragmentation of LECs in RT control and *shi*<sup>ts</sup> expressing LECs**

Live imaging of the FRET ratio of the nuclear localized SCAT3 caspase activation indicator (ECFP/Venus) for RT control LECs under the restrictive temperature. The higher FRET ratio indicates the higher caspase activity. Dorsal view. Anterior is up. Scale bar: 50  $\mu$ m. Time interval: 100 sec.



**Movie 11. Caspase activation is observed before fragmentation of LECs in *shi<sup>ts</sup>* expressing LECs**

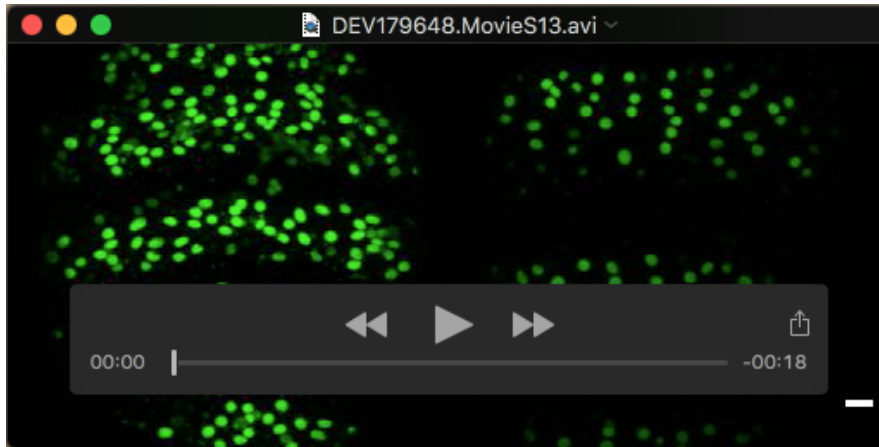
Live imaging of the FRET ratio of the nuclear localized SCAT3 caspase activation indicator (ECFP/Venus) for *shi<sup>ts</sup>* expressing LECs under the restrictive temperature. The higher FRET ratio indicates higher caspase activity. Dorsal view. Anterior is up. Scale bar: 50  $\mu$ m. Time interval: 100 sec.



**Movie 12. Over-expression of *DIAP1* suppresses cell elimination caused by expressing *shi<sup>ts</sup>* in the LECs**

Live imaging of LEC elimination from pupae under the restrictive temperature for *shi<sup>ts</sup>* expressing (left) and *DIAP1* and *shi<sup>ts</sup>* expressing (right) pupae. Dorsal view. Anterior is up. Scale bar: 50  $\mu$ m. Time interval: 10 min.





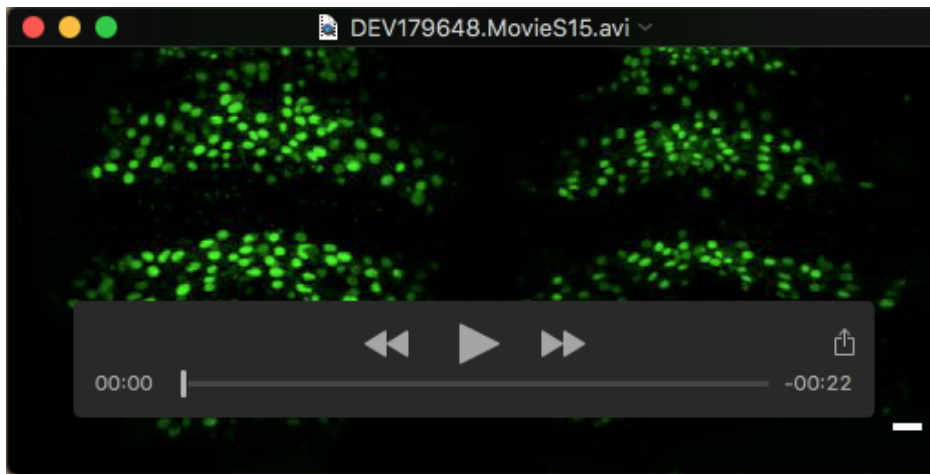
**Movie 13. Induction of *E-cadherin* RNAi in the LECs promotes cell elimination**

Live imaging of LEC elimination for control (left) and *E-cadherin* RNAi (right) LECs at 25°C. Dorsal view. Anterior is up. Scale bar: 50 μm. Time interval: 10 min.



**Movie 14. Over-expression of *DIAP1* suppresses cell elimination caused by the reduction of *E-cadherin* in the LECs**

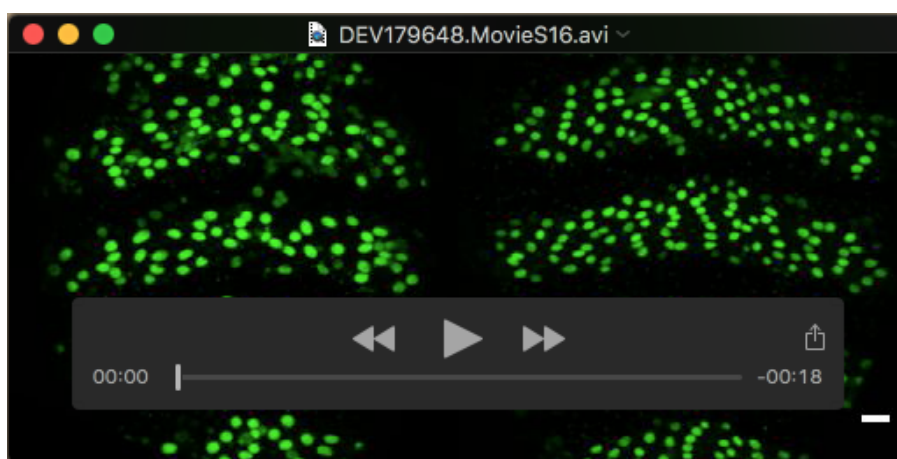
Live imaging of the LEC elimination for control (left) and *DIAP1* and *E-cadherin* RNAi (right) LECs at 25°C. Dorsal view. Anterior is up. Scale bar: 50 μm. Time interval: 10 min.



**Movie 15. Over-expression of *E-cadherin* moderates increased cell elimination caused by expressing *shi*<sup>ts</sup> in the LECs**

Live imaging of LEC elimination under the restrictive temperature for *shi*<sup>ts</sup> expressing (left) and *shi*<sup>ts</sup> and *E-cadherin* over-expressing (right) LECs. Dorsal view. Anterior is up.

Scale bar: 50  $\mu$ m. Time interval: 10 min.



**Movie 16. Induction of *Rab7* RNAi in the LECs promotes cell elimination**

Live imaging of LEC elimination for control (left) and *Rab7* RNAi (right) LECs at 25°C.

Dorsal view. Anterior is up. Scale bar: 50  $\mu$ m. Time interval: 10 min.